INFLAMMATION

Enhancement of Regnase-1 expression with stem loop–targeting antisense oligonucleotides alleviates inflammatory diseases

Ka Man Tse[1], Alexis Vandenbon[2], Xiaotong Cui[1], Takashi Mino[1], Takuya Uehata[1], Keiko Yasuda[1], Ayuko Sato[3], Tohru Tsujimura[3], Fabian Hia[1], Masanori Yoshinaga[1], Makoto Kinoshita[4], Tatsusada Okuno[4], Osamu Takeuchi[1]*

Regnase-1 is an ribonuclease that plays essential roles in restricting inflammation through degrading messenger RNAs (mRNAs) involved in immune reactions via the recognition of stem-loop (SL) structures in the 3′ untranslated regions (3′UTRs). Dysregulated expression of Regnase-1 is associated with the pathogenesis of inflammatory and autoimmune diseases in mice and humans. Here, we developed a therapeutic strategy to suppress inflammatory responses by blocking Regnase-1 self-regulation, which was mediated by the simultaneous use of two antisense phosphorodiamidate morpholino oligonucleotides (MOs) to alter the binding of Regnase-1 toward the SL structures in its 3′UTR. Regnase-1–targeting MOs not only enhanced Regnase-1 expression by stabilizing mRNAs but also effectively reduced the expression of multiple proinflammatory transcripts that were controlled by Regnase-1 in macrophages. Intratracheal administration of Regnase-1–targeting MOs ameliorated acute respiratory distress syndrome and chronic fibrosis through suppression of inflammatory cascades. In addition, intracranial treatment with Regnase-1–targeting MOs attenuated the development of experimental autoimmune encephalomyelitis by promoting the expansion of homeostatic microglia and regulatory T cell populations. Regnase-1 expression was inversely correlated with disease severity in patients with multiple sclerosis, and MOs targeting human *Regnase-1* SL structures were effective in mitigating cytokine production in human immune cells. Collectively, MO-mediated disruption of the Regnase-1 self-regulation pathway is a potential therapeutic strategy to enhance Regnase-1 abundance, which, in turn, provides therapeutic benefits for treating inflammatory diseases by suppressing inflammation.

INTRODUCTION

Posttranscriptional regulation of gene expression has a crucial role in fine-tuning inflammatory responses by regulating the stability and translation of mRNAs encoding cytokines and other inflammatory mediators (*1*–*3*). Inflammatory mRNAs are tightly controlled through the recognition of cis-elements such as stem-loop (SL) structures and AU-rich elements present in the 3′ untranslated regions (3′UTRs) by RNA binding proteins (RBPs) such as Regnase-1 (also known as Zc3h12a and MCPIP1), Roquin-1/2, and Tristetraprolin (TTP) (*3*). Regnase-1 is an RBP that has a ribonuclease domain and a CCCH-type zinc finger domain (*4*). Regnase-1 degrades inflammation-related mRNAs, such as *Il6*, *Il1b*, and *Il12p40* in macrophages, in response to Toll-like receptor (TLR) stimulation, and can target T cell activation transcripts such as *Icos*, *Rel*, and *Il2* through its endoribonuclease activity (*4*–*6*). Regnase-1 binds to SL structures with a pyrimidine-purine-pyrimidine (Py-Pu-Py) loop sequence present in the 3′UTRs of target mRNAs, and this allows for the association of helicase UPF1 after termination of translation, upon which UPF1 unwinds the SL structures for cleavage by Regnase-1 (*7*, *8*). *Regnase-1*–deficient mice spontaneously develop autoimmune inflammatory diseases, suggesting that Regnase-1 plays a critical role in the maintenance of immune homeostasis (*4*, *6*, *9*, *10*). Moreover, Regnase-1 is involved in the development of human inflammatory diseases, including ulcerative colitis and idiopathic pulmonary fibrosis (IPF) (*11*–*13*), and together, these observations suggest that Regnase-1 is a potential therapeutic target. Strategies designed to modulate the availability of Regnase-1 may be able to curb immune responses and inflammation. Whereas depletion of Regnase-1 in T cells was reported to enhance antitumor immunity (*14*), therapeutic approaches to increase Regnase-1 as a strategy to treat inflammatory diseases have not been established.

Antisense oligonucleotides (ASOs) are short, single-stranded synthetic nucleotides that can bind to target RNAs via complementary base pairs (*15*). These molecules have been widely used to modulate mRNA stability by various mechanisms including (i) lowering mRNA or protein abundance through ribonuclease (RNase) H1 recruitment (*16*) or sterically blocking translation of mature mRNAs (*17*), (ii) altering mRNA splicing patterns (*18*–*20*), and (iii) inhibiting the function of microRNAs or other small RNAs (*21*). In addition, several in vivo delivery methods have been proven to be effective for organ-specific distribution of ASOs (*22*). To enhance the pharmacokinetics and biodistribution of ASOs, strategies such as chemical modifications of the ribose sugars, including 2′-*O*-methyl (2′-OMe); bridged nucleic acid (BNA) modifications; and usage of phosphorodiamidate morpholino oligonucleotide (MO) backbone linkages have been applied to current ASO technology (*23*). Because of their high stability and versatility, MO-based ASOs were clinically approved for the treatment of spinal muscular atrophy and Duchenne muscular dystrophy in 2016 and 2019 (*19*, *20*).

[1]Department of Medical Chemistry, Graduate School of Medicine, Kyoto University, Kyoto, Kyoto 606-8501, Japan. [2]Institute for Frontier Life and Medical Sciences, Kyoto University, Kyoto, Kyoto 606-8501, Japan. [3]Department of Pathology, Hyogo College of Medicine, Nishinomiya, Hyogo 663-8501, Japan. [4]Department of Neurology, Graduate School of Medicine, Osaka University, Suita, Osaka 565-0871, Japan. *Corresponding author. Email: otake@mfour.med.kyoto-u.ac.jp

The expression of *Regnase-1* mRNA is negatively regulated by Regnase-1–mediated mRNA degradation via the SL structures in its own 3′UTR (*5*). Thus, we hypothesized that modulating the SL motif itself could be an advantageous approach to restrict Regnase-1 self-regulation, thereby increasing *Regnase-1* mRNA and, subsequently, protein availability. We evaluated the ability of antisense MOs to bind to Regnase-1 SL structures and affect Regnase-1 mRNA stability. Treatment of cells with Regnase-1–targeting MOs resulted in *Regnase-1* mRNA stabilization and increased the potency of Regnase-1 in degrading inflammatory transcripts. Furthermore, our in vivo data provided evidence for the therapeutic potential of Regnase-1–targeting MOs in hampering the progression of a number of disease models in which inflammation is a driving force, including an acute lung injury model, a chronic lung fibrosis model and the experimental autoimmune encephalomyelitis (EAE) model.

RESULTS

SL-modifying MOs suppress Regnase-1 self-regulation

We previously identified an SL sequence in mouse *Regnase-1* (*Zc3h12a*) 3′UTR (194–211) that contributes to the Regnase-1 self-degradation (*5*). To screen for additional motifs in the *Regnase-1* 3′UTR (1–865), we constructed luciferase reporters harboring different regions of the mouse *Regnase-1* 3′UTR. Regnase-1 destabilized its own mRNAs via two independent regions: 1–210 and 363–516 (Fig. 1A). In contrast, expression of the nuclease-inactive mutant of Regnase-1 (D141N) failed to suppress the reporter activity, indicating that the ability of Regnase-1 to self-regulate was dependent on its nuclease function (Fig. 1A). In addition to region 196–210, the 379–391 region was also predicted to form an SL structure (fig. S1A). These two SL regions are evolutionally well conserved and harbor a common Py-Pu-Py sequence in the loop region (Fig. 1B and fig. S1A). Addition of these two SL motifs to the pGL3-β-globin 3′UTR conferred RNase-dependent responsiveness to Regnase-1 (Fig. 1B). Whereas the reporter harboring *Regnase-1* 3′UTR was highly unstable compared with the control, disruption of single SL structure by substitution mutations (196–210: SL1 mutant and 379–391: SL2 mutant) stabilized the reporters, and mutations of both SLs further increased the luciferase activity (Fig. 1C), highlighting the importance of the two SL motifs in the control of Regnase-1 self-regulation.

These results prompted us to manipulate the SL structures in the *Regnase-1* 3′UTR to specifically control its mRNA stability. To this end, we examined the idea of repurposing the antisense phosphorodiamidate MOs to alter the binding of the two SL sequences to Regnase-1, which is in contrast to the conventional mechanism of action of ASOs (*24*). We designed two MOs to partially overlap the right arm of each stem sequence at the 3′UTR of mouse *Regnase-1* (Fig. 1D). As controls, we used saline or control MO (Ctrl MO), which lacks any specific target within the murine transcriptome. To verify the effectiveness of the designed MOs to alter the Regnase-1–mediated self-regulation, we examined the activity of a luciferase reporter harboring mouse *Regnase-1* 3′UTR after treatment with Ctrl MO, MO targeting Regnase-1 SL1 or SL2 (MO1 or MO2) or both SLs (MO1 + MO2) in HeLa cells. As shown in Fig. 1E, individual treatment of cells with MO1 and MO2 increased the luciferase stability of the *Regnase-1* 3′UTR. This could be further increased upon treatment with the MO cocktail (MO1 + MO2), indicating that the combined use of MO1 and MO2 conferred the highest stability toward *Regnase-1* mRNA. In addition, treatment of MO1 and MO2 simultaneously abolished the degradation of luciferase mRNAs harboring the 3′UTR of *Regnase-1*, but not *Il6* [which harbors Regnase-1–specific SL structure in 3′UTR region 84–102 (*4*, *7*)], likely induced by Regnase-1 overexpression (Fig. 1F). This result confirmed that the effect of Regnase-1–targeting MOs was through the suppression of Regnase-1–mediated mRNA decay. Only MOs interfering with SL formation (left arm or right arm), but not ones targeting regions outside the SL sequence, exerted the observed stabilization effect (fig. S1B). Furthermore, MO cocktail treatment did not further increase the luciferase activity in reporters harboring selective mutations in the SL sequences of *Regnase-1* 3′UTR (Fig. 1G), suggesting that the increased mRNA stability by MO cocktail is through the alteration of the SL structures and thus excludes the possibility of off-target effects.

The two SL structures are highly conserved among mammals including humans (fig. S1A), so we investigated whether interfering with SL formation could also be effective in blocking Regnase-1 self-regulation in humans. The human *Regnase-1* 3′UTR also adopts two SL structures, and these structural motifs conferred *Regnase-1* mRNA instability in humans (Fig. 1, H and I). Similarly, mutations disrupting SL1 and SL2 abolished the self-regulation ability of human Regnase-1 (fig. S1C). MOs designed to disrupt the SLs in human *Regnase-1* 3′UTR showed similar stabilization effects on the luciferase reporter–based gene expression assays (fig. S1, D and E). These data together confirmed that MO cocktail treatment could block the Regnase-1–mediated self-regulation in both mouse and human.

To investigate the underlying mechanism of Regnase-1–targeting MOs in suppressing Regnase-1 self-degradation, we performed RIP assay in HeLa cells expressing the Flag-Regnase-1 D141N mutant. Reverse transcription quantitative polymerase chain reaction (RT-qPCR) analysis of the eluted mRNAs revealed that Regnase-1–targeting MOs reduced the association of Regnase-1 to its mRNA without affecting its binding to *IL6* mRNA (Fig. 1J; Flag-Regnase-1, 72 kDa; β-actin, 42 kDa). These results indicate that Regnase-1–targeting MOs are effective in conferring resistance to Regnase-1–mediated self-degradation by altering the binding efficiency of Regnase-1 toward the SL structural motifs present in its 3′UTR.

Regnase-1–targeting MOs attenuated inflammatory responses in macrophages by augmenting Regnase-1 expression

We evaluated whether we could manipulate the abundance of *Regnase-1* mRNA using Regnase-1–targeting MOs in innate immune cells. Consistent with the inhibition of Regnase-1 self-regulation, treatment of murine bone marrow–derived macrophages (BMDMs) with MO1 or MO2 modestly increased *Regnase-1* mRNA, whereas the combination of MO1 and MO2 (hereafter Reg1-MOs) markedly increased *Regnase-1* mRNA expression (Fig. 2A). Reg1-MOs enhanced the abundance of *Regnase-1* transcripts in Raw264.7 cells and mouse peritoneal macrophages (fig. S2, A and B), and immunoblot analysis revealed that Regnase-1 protein expression was greatly enhanced by Reg1-MO treatment in BMDMs (Fig. 2B; Regnase-1, 72 kDa; β-actin, 42 kDa). BMDMs were capable of MO uptake with a transfection efficiency of 97% over a 72-hour period (fig. S2C), and Reg1-MOs did not affect cell viability (fig. S2, D and E).

We examined the effects of Reg1-MO–mediated increase in Regnase-1 in inflammatory responses in innate immune cells. Treatment of BMDMs with Reg1-MOs resulted in a robust increase in *Regnase-1* mRNA expression in a dose-dependent manner (Fig. 2C). The expression of *Regnase-1* is inducible by the TLR4 ligand

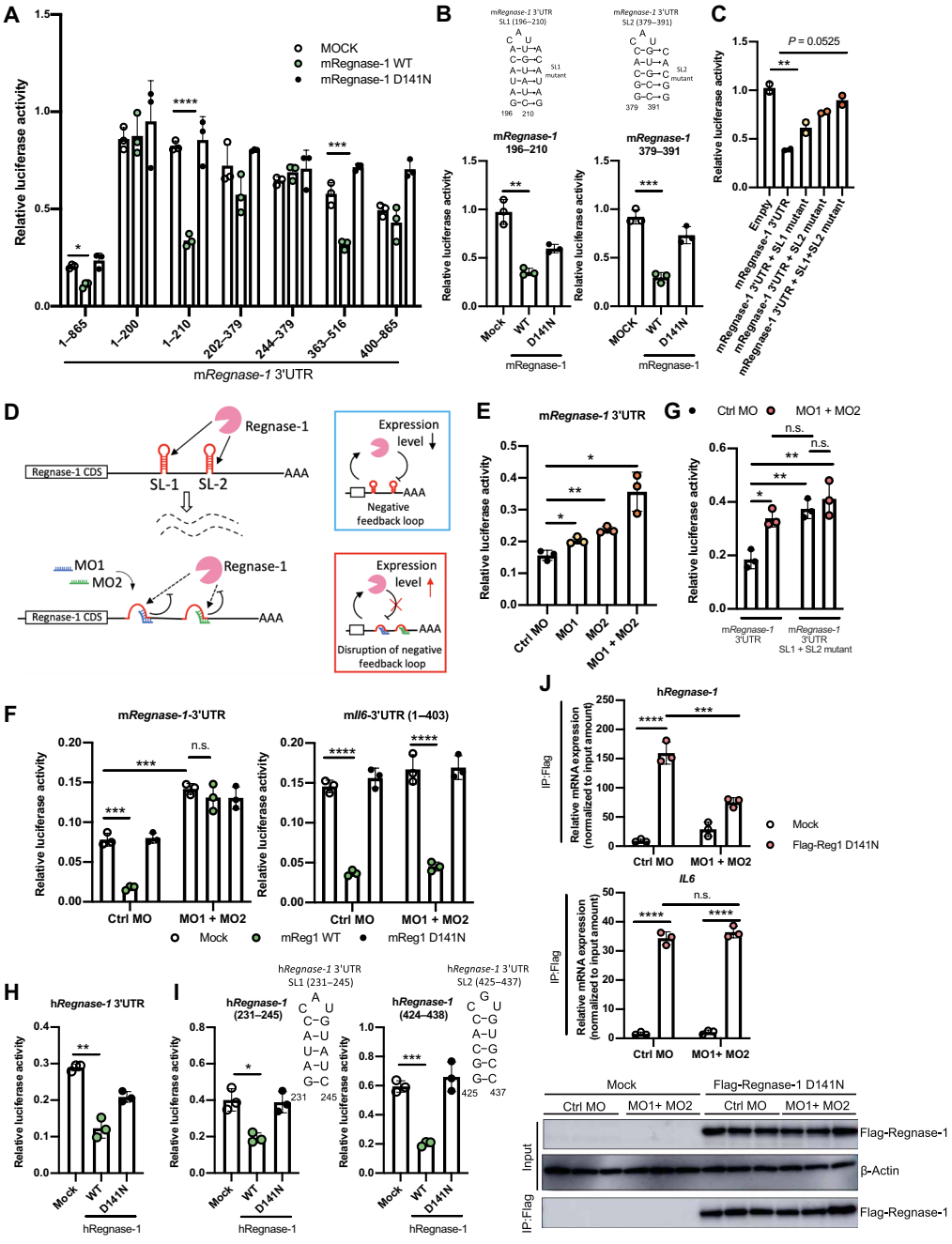

Fig. 1. Identification of SL motifs in m*Regnase-1* 3′UTR and the manipulation of their stability by MOs. (**A** and **B**) Luciferase activity of HeLa cells transfected with the indicated pGL3 reporters, together with the control (mock), wild-type (WT), or D141N nuclease-dead mutant of Regnase-1 expression plasmids ($n = 3$), and the schematic representation of Regnase-1's SL structures and the respective stem mutants. (**C**) Luciferase activity of HeLa cells transfected with the indicated mutant pGL3 reporters and Regnase-1 expression plasmids ($n = 2$). (**D**) Regnase-1 self-degradation pathway and the proposed mechanism of action of MO1 and MO2. (**E**) Luciferase activity of HeLa cells transfected with pGL3 reporter containing m*Regnase-1* 3′UTR, together with control MO, MO1, MO2, or MO1 and MO2 ($n = 3$). (**F**) Luciferase activity of HeLa cells transfected with pGL3-plasmid containing m*Regnase-1* 3′UTR and m*Il6* 3′UTR, Ctrl MO or MO1 and MO2, and Regnase-1 expression plasmids ($n = 3$). (**G**) Luciferase assay of HeLa cells transfected with the indicated pGL3 reporters, together with Ctrl MO or Reg1-MOs ($n = 3$). (**H** and **I**) Luciferase activity of HeLa cells transfected with pGL3 reporter containing h*Regnase-1* 3′UTR and Regnase-1 expression plasmids ($n = 3$), and the schematic representations of stem-loop structure in h*Regnase-1* mRNA. (**J**) RIP RT-qPCR analysis of the eluted RNAs from HeLa cells transfected with pcDNA3.1(+) or Regnase-1 D141N expression plasmids, together with Ctrl MO or MO1 + MO2 ($n = 3$). Immunoblot analysis of Flag-Regnase-1 (72 kDa) obtained from total cell lysate or coimmunoprecipitated with the RNA from the indicated experiment groups (β-actin: 42 kDa). All luciferase activities were shown as relative values. Error bars indicate means ± SD. *$P \leq 0.05$; **$P \leq 0.01$; ***$P \leq 0.001$; ****$P \leq 0.0001$; n.s., not significant.

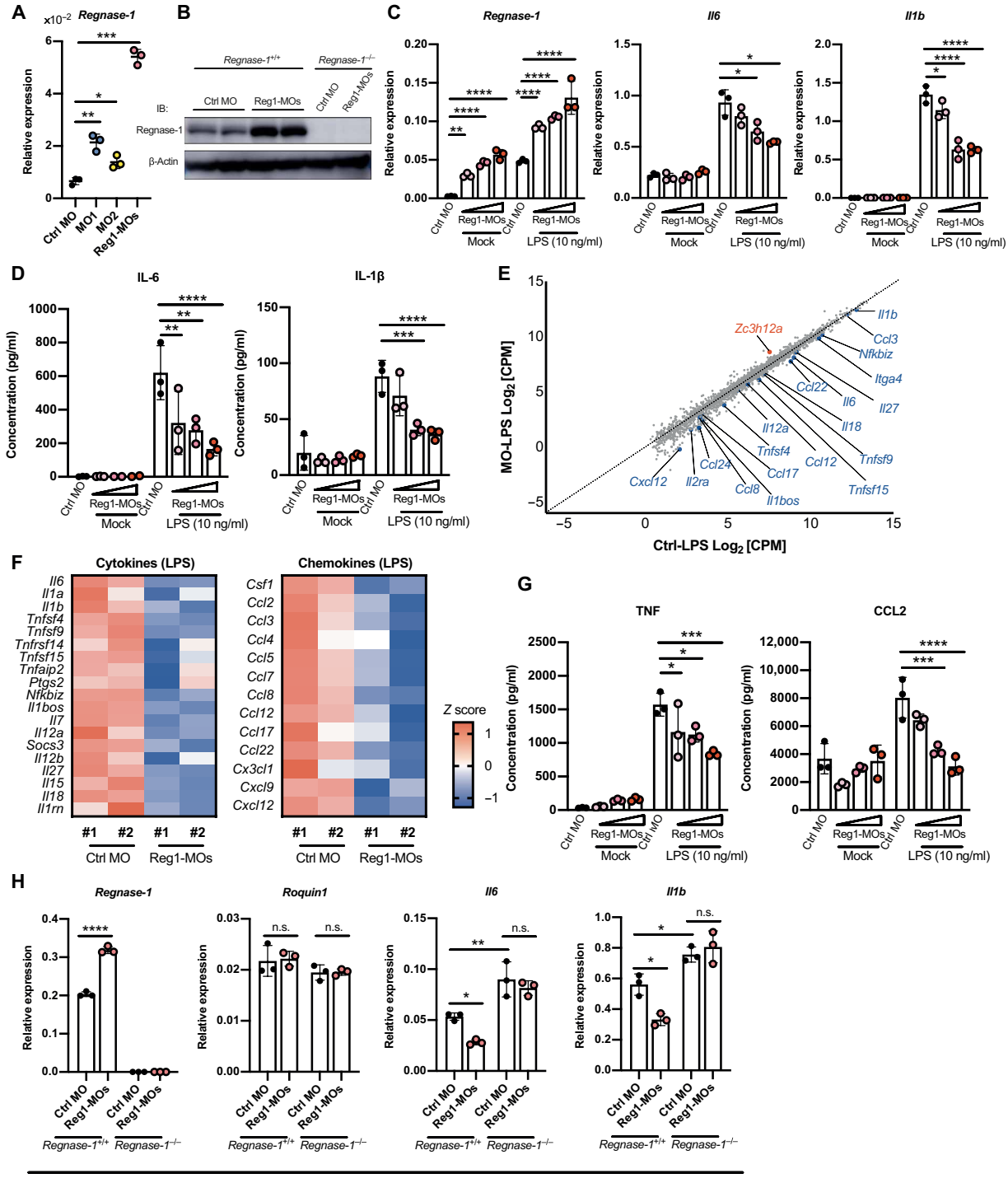

Fig. 2. Blockage of Regnase-1 self-degradation by Reg1-MOs ameliorated inflammations. (**A**) RT-qPCR analyses of *Regnase-1* expression in BMDMs transfected with Ctrl MO, MO1, MO2, or Reg1-MOs for 24 hours ($n = 3$). (**B**) Immunoblot analysis of Regnase-1 in *Regnase-1*$^{+/+}$ and *Regnase-1*$^{-/-}$ BMDMs transfected with Ctrl MO or Reg1-MOs ($n = 2$ for *Regnase-1*$^{+/+}$ BMDMs and $n = 1$ for *Regnase-1*$^{-/-}$ BMDMs; Regnase-1: 72 kDa, β-actin: 42 kDa). (**C**) RT-qPCR analyses of the indicated genes in BMDMs transfected with Ctrl MO or Reg1-MOs in different concentrations (1, 3, and 6 μM) in the presence or absence of LPS ($n = 3$). (**D** and **G**) Protein levels of IL-6, IL-1β, TNF, and CCL2 in the cell culture supernatants collected from BMDMs transfected with Ctrl MO or Reg1-MOs in different concentrations in the presence or absence of LPS ($n = 3$). (**E**) Scatter plot of Log_2 CPM value between Ctrl MO–treated (*x* axis) and Reg1-MO–treated BMDM samples (*y* axis). Genes of interest found up-regulated or down-regulated were labeled in red and blue, respectively. (**F**) Heatmap representations depicting the expression of inflammatory transcripts in Ctrl MO– or Reg1-MO–treated BMDMs stimulated with LPS (red indicates up-regulated, blue represents down-regulated; $n = 2$ per group). *Z* scores were plotted for each gene. (**H**) RT-qPCR analyses of the indicated genes in *Regnase-1*$^{+/+}$ and *Regnase-1*$^{+/-}$ BMDMs transfected with Ctrl MO or Reg1-MOs in the presence of LPS (100 ng/ml; $n = 3$). Error bars indicate means ± SD. $^{*}P \le 0.05$; $^{**}P \le 0.01$; $^{***}P \le 0.001$; $^{****}P \le 0.0001$.

lipopolysaccharide (LPS) (*5*), and we observed that *Regnase-1* expression was further increased upon administration of Reg1-MOs with LPS (Fig. 2C). In contrast, Reg1-MOs suppressed the expressions of *Il6* and *Il1b* on both mRNA and protein levels in response to LPS in a dose-dependent manner (Fig. 2, C and D). To further evaluate the global gene expression changes associated with Reg1-MO treatment, we performed RNA sequencing (RNA-seq) analysis of LPS-stimulated BMDMs pretreated with Ctrl MO or Reg1-MOs. Transcriptomic profiling revealed 562 differentially expressed genes between the Ctrl and Reg1-MO groups (Fig. 2E, fig. S3A, and data file S1). Among them, 273 genes showed increased expression upon treatment with Reg1-MOs (hereafter "up-regulated genes") (Fig. 2E and fig. S3A). *Zc3h12a* (*Regnase-1*, $\log_2$FC, 1.1; P_{adj}, 3.91×10^{-5}; fig. S3B) was one of the most markedly up-regulated genes upon Reg1-MO treatment, among the RBPs involved in the mechanism of mRNA decay (fig. S3C) (*1*, *25*). Gene ontology (GO) enrichment analysis showed that genes categorized as "negative regulation of IL-6 production," and "negative regulation of TNF production" were enriched in the up-regulated genes (fig. S3D and data file S2). In contrast, GO analysis of 289 genes decreased by treatment with Reg1-MOs (hereafter "down-regulated genes") revealed that genes associated with the biological processes such as "cellular response to chemokines" and "inflammatory responses" were enriched (data file S3). Inflammation-related cytokines and chemokines, but not anti-inflammatory cytokines, were down-regulated in BMDMs treated with Reg1-MOs (Fig. 2F and fig. S3E). Nevertheless, Reg1-MOs did not affect the expression of *Ifnb* or other interferon (IFN)–stimulated genes (fig. S3F), suggesting Reg1-MOs did not elicit nonspecific IFN responses. Reg1-MO–mediated suppression of cytokines and chemokine-related molecules in BMDMs was further confirmed (fig. S3G). Consistently, Reg1-MO treatment effectively suppressed the production of tumor necrosis factor (TNF) and CCL2 in LPS-stimulated BMDMs (Fig. 2G). In contrast, Reg1-MOs failed to decrease the cytokine expressions in *Regnase-1*–deficient BMDMs, confirming that Reg1-MOs suppressed TLR-induced inflammatory gene expression specifically through the control of Regnase-1 turnover (Fig. 2H).

Treatment of Reg1-MOs suppressed acute lung inflammation in mice

These results prompted us to investigate whether Reg1-MOs exhibit therapeutic effect against inflammatory diseases in vivo. For the administration of Reg1-MOs in vivo, we used vivo-MO consisting of MOs conjugated with a covalently linked delivery moiety (guanidinium group) (*26*). We found that intratracheal treatment of Reg1-MOs efficiently increased the abundance of mRNAs encoding *Regnase-1*, but not *Roquin-1*/*2*, in lung tissue (Fig. 3A). Treatment of mice with Reg1-MOs did not cause observable toxicity to the mice, as evaluated by the body weight change (fig. S4A).

We evaluated the LPS-induced acute respiratory distress syndrome (ARDS) model, because *Regnase-1*$^{+/-}$ mice intratracheally challenged with LPS exhibited increased lung–to–body weight ratio, elevated infiltration of Gr1$^+$F4/80$^-$ neutrophils in lungs, and enhanced expression of proinflammatory cytokines (*Il6* and *Il1b*), compared to their wild-type (WT) counterparts (fig. S4, B to D). These findings indicated that reduction in Regnase-1 levels exacerbated LPS-induced inflammation in the lung.

To evaluate the in vivo therapeutic efficacy of Reg1-MOs in counteracting ARDS induced by LPS, mice were administrated with Ctrl MO (Ctrl group) or vivo-MOs targeting the two *Regnase-1* SLs (Reg1-MO group) 24 hours before the LPS challenge (Fig. 3B). Examination of inflammation status 6 hours after LPS administration revealed a marked increase in the total inflammatory cell counts in lung tissue and bronchoalveolar lavage (BAL) fluid in the Ctrl group, mainly attributable to neutrophil migration to the lung (Fig. 3, C and D). Treatment of mice with Reg1-MOs significantly reduced the total cell and neutrophil counts in the lung tissue and BAL fluid (Fig. 3, C and D; $P \leq 0.01$). Histological examination of lung tissues revealed that the LPS-induced increase in inflammatory cells in the alveolar space and interalveolar septal thickening was markedly alleviated in the Reg1-MO group (Fig. 3E), as revealed by the lung injury score (Fig. 3F). Furthermore, Reg1-MO treatment reduced the expression of proinflammatory cytokines (*Il6*, *Il1b*, and *Tnf*) but not anti-inflammatory cytokines in the lung tissues in response to the LPS challenge (Fig. 3G and fig. S4E).

Alveolar macrophages (AMs) are critical regulators of the lung inflammatory response and are key contributors in the progression of acute lung injury (*27*, *28*). We found that the AMs derived from the Reg1-MO group not only showed an increase in *Regnase-1* expression but also exhibited a trend of reduced expression of proinflammatory cytokines and neutrophil chemoattractants (*7*) that are targets of Regnase-1 (fig. S4F), suggesting that the improved lung architecture and impaired neutrophil recruitment to sites of inflammation were due, in part, to a decrease in inflammatory and chemotactic signals secreted by AMs.

Administration of Reg1-MOs alleviated lung fibrosis in mice

Next, we tested the anti-inflammatory aspects of Reg1-MOs in resolving complications because of chronic inflammation. Lung fibrosis is caused by prolonged inflammatory responses in the lung tissue (*29*–*31*). Regnase-1–mediated restriction of type 2 cytokine transcripts in group 2 innate lymphoid cells (ILC2s) regulates fibrosis development in the bleomycin-mediated lung fibrosis model, and lower expression of Regnase-1 correlated with increased ILC2 numbers and was associated with a poor prognosis in patients with IPF (*13*). Concomitantly, *Regnase-1*$^{+/-}$ mice suffered more severe inflammatory and fibrotic symptoms than WT mice in a bleomycin-induced lung fibrosis model (fig. S5, A to C). Thus, we tested whether enhancing the availability of Regnase-1 in the lung would limit pulmonary fibrosis.

We intratracheally treated mice with Ctrl MO or Reg1-MOs every 8 days for 16 days (days 0, 8, and 16), instilled bleomycin in the lung on day 3, and harvested the tissues on day 24 (Fig. 4A). The body weight changes were comparable between the Ctrl and Reg1-MO groups during the course of disease development (fig. S5D), but infiltration of immune cells, especially neutrophils, CD4$^+$ T cells, and ILC2 numbers was markedly decreased in the lung tissues of the Reg1-MO group (Fig. 4, B and C). Histological analysis revealed a marked decrease in inflammatory cell infiltration and cellular injury and fibrotic lesion in the lungs of mice treated with the Reg1-MOs (Fig. 4, D and E). The expression of anti-inflammatory transcripts remained unchanged (fig. S5E), but the bleomycin-induced expression of fibrotic markers Collagen 1α, Collagen 3α, and fibronectin was repressed in the lungs of Reg1-MO group (Fig. 4F).

Various types of pulmonary cells can drive the development of lung fibrosis, but AMs are known to be crucial regulators of fibrosis by producing inflammatory and profibrotic mediators (*32*, *33*). Thus, we isolated AMs from prefibrotic lungs derived from Ctrl and Reg1-MO animals 7 days after bleomycin treatment insult and

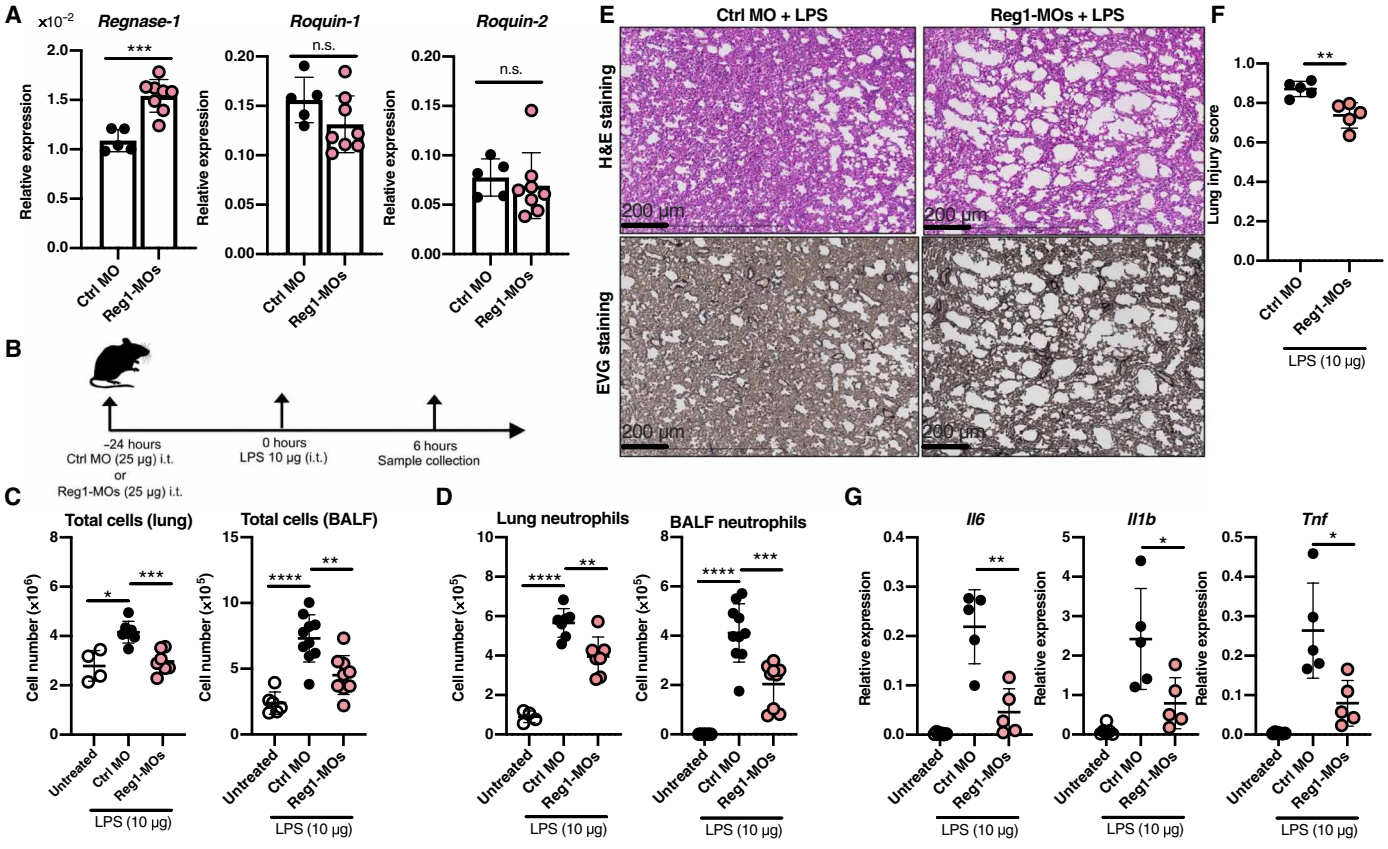

Fig. 3. Reg1-MO treatment blunted inflammation in an acute lung inflammation model. (**A**) RT-qPCR analyses of *Regnase-1* and *Roquin-1/2* in lung tissues from mice that received intratracheal treatment with Ctrl MO or Reg1-MOs ($n = 5$ for Ctrl group and $n = 8$ for Reg1-MO group). (**B**) Schematic of the workflow of Reg1-MO treatment in LPS-induced ARDS model. (**C** and **D**) Total cell number and neutrophil influx in the lung tissue and bronchoalveolar lavage (BAL) fluid in untreated and LPS-treated B6 mice that received Ctrl MO or Reg1-MO treatment ($n = 4$ to 6 for untreated animals, $n = 7$ to 10 for LPS-treated animals given Ctrl MO or Reg1-MO treatment). (**E**) Representative images of lung tissue from each experimental group observed by hematoxylin and eosin staining (H&E; top) and Verhoeff Van Gieson staining (EVG; bottom). Scale bars, 200 μm. (**F**) Statistical analysis of the lung injury score in lung tissues derived from each experimental group ($n = 5$ for LPS-treated animals that received Ctrl MO or Reg1-MO treatment). (**G**) RT-qPCR analyses for the indicated genes in the lung homogenates of each experimental group ($n = 6$ for untreated, $n = 5$ for LPS-treated animals that received Ctrl MO or Reg1-MO treatment). Error bars indicate means ± SD. $^*P \le 0.05$; $^{**}P \le 0.01$; $^{***}P \le 0.001$; $^{****}P \le 0.0001$.

compared their gene expression differences by RT-qPCR. We found that Reg1-MO treatment repressed the expression of proinflammatory cytokines and chemokines as well as their ligands in AMs, accompanied by an enhancement of *Regnase-1* expression (fig. S5F). Together, these results suggested that Reg1-MO–mediated enhancement of *Regnase-1* in AMs inhibited the chronic inflammatory and fibrotic actions imposed by bleomycin, resulting in an amelioration of fibrosis.

Intracranial treatment of Reg1-MOs impeded EAE development

Reg1-MOs appear to be potent suppressants of both acute and chronic inflammatory diseases, so we next examined whether this approach could be applied to the treatment of autoimmune diseases caused by a defect in immune tolerance. We used the EAE mouse model, an animal equivalent of the human multiple sclerosis (MS) disease, characterized by demyelination in the central nervous system (CNS) (*34*). Consistent with a previous report, *Regnase-1*$^{+/-}$ mice displayed exacerbated CNS inflammation and clinical pathology compared with WT animals after active induction of EAE (fig. S6A) (*35*).

Reg1-MOs were delivered to the CNS via intracranial injection to bypass the blood-brain barrier, and an enhancement of the CNS *Regnase-1* expression was confirmed (fig. S6B). We intracranially treated mice with Reg1-MOs 9 days after EAE immunization and found that single administration of Reg1-MOs in EAE mice attenuated the disease severity, with significant delay in disease onset (Fig. 5A; $P \le 0.05$ on days 11 to 24), better weight recovery, and lower incidence of paralysis (fig. S6C). Histological examination revealed lower infiltration of immune cells and reduced demyelination events in the spinal cord of the Reg1-MO group (Fig. 5, B and C). Consistently, there was a decrease in the expression of proinflammatory cytokines and chemokines involved in recruitment of monocytes and neutrophils (*Cxcl1*, *Cxcl2*, *Cxcl5*, *Ccl2*, and *Ccl4*) in the spinal cord of Reg1-MO–treated EAE mice (Fig. 5D and fig. S6D).

To further clarify the cell types responsible for the suppression of autoimmune responses, single-cell RNA-seq (scRNA-seq) on CD45$^+$ cells isolated from spinal cords of Ctrl and Reg1-MO mice was performed (fig. S7A and table S1). Unsupervised clustering analysis revealed 24 distinct immune cell subsets in EAE mice (Fig. 5E and figs. S7B and S8, A and B). CD45$^+$ cells from the Ctrl and Reg1-MO groups showed similar cellular distributions, but we found marked decreases in all neutrophil and inflammatory monocyte subsets, and reciprocal increase in Foxp3$^+$ regulatory T cell

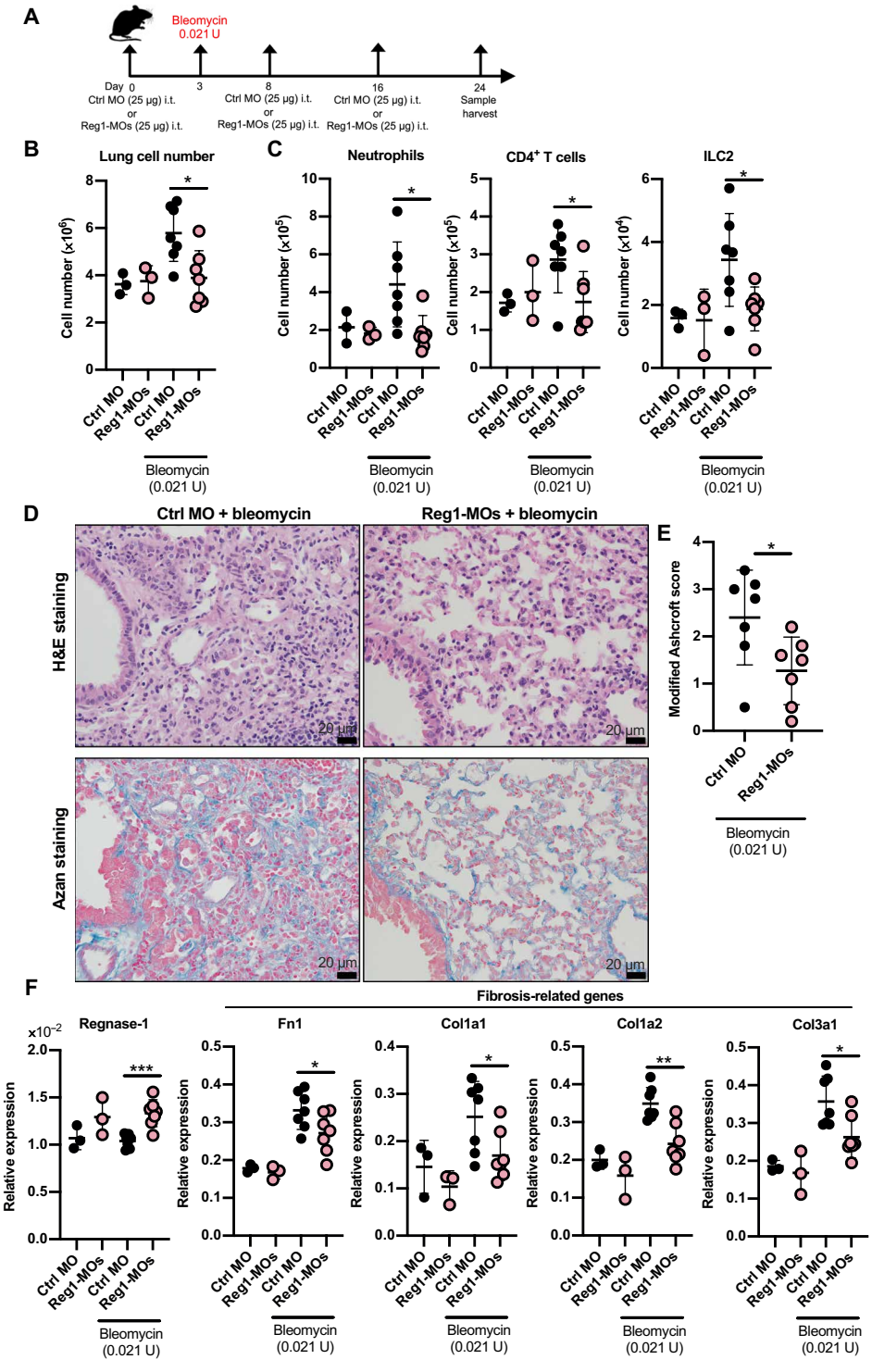

Fig. 4. Reg1-MOs attenuated the clinical severity of lung fibrosis by enhancing Regnase-1 availability. (**A**) Schematic of the workflow of Reg1-MO treatment in bleomycin-induced lung fibrosis model. (**B**) Total cell number, (**C**) flow cytometry analyses of cellular influx, and (**F**) RT-qPCR analyses for the indicated genes in the lung tissue from B6 mice receiving repeated intratracheal administration of Ctrl MO or Reg1-MOs treated with or without 0.021 U of bleomycin ($n = 3$ for mice administrated with Ctrl MO or Reg1-MOs, $n = 7$ for bleomycin-treated mice administrated with Ctrl MO or Reg1-MOs). (**D**) Representative images of lung tissues observed by H&E staining (top) and Azan staining (bottom) of lung sections from the indicated bleomycin-treated animals. Scale bars, 20 μm. (**E**) Modified Ashcroft score in the lung homogenates from the indicated groups of bleomycin-treated animals ($n = 7$ for each group). Error bars indicate means ± SD. *$P \leq 0.05$; **$P \leq 0.01$; ***$P \leq 0.001$.

(T_{reg}) and homeostatic microglia subsets (Fig. 5F and fig. S9, A and B). Consistently, flow cytometry analyses showed substantial reduction of neutrophils and Ly6C^{hi} monocytes in the spinal cord infiltrates of Reg1-MO–treated EAE animals (Fig. 5G). These data indicated that intracranial administration of Reg1-MOs restricted the infiltration of a set of immune cells to spinal cords during EAE development.

Subsets of CD4$^+$ T cells secreting IFNγ and interleukin-17A (IL-17A) were considerably lower in the spinal cord of the Reg1-MO group (Fig. 5G). Given the pronounced pathogenic roles of type 1 T helper (T_H1, IFNγ$^+$) and T_H17 cells (IL-17A$^+$) in EAE (*36*–*38*), we studied the cytokine response in CD4$^+$ T cells upon administration of Reg1-MOs in more detail. We observed that Reg1-MO treatment not only increased *Regnase-1* expression in naïve CD4$^+$ T cells (fig. S10A) but also reduced the frequencies of IFNγ$^+$ and IL-17A$^+$ cells in a dose-dependent manner (Fig. 5H and fig. S10, B to D). Given a major role of IL-17A in neutrophil infiltration and activation (*39*), we reasoned that the observed lower immune cell infiltration to the CNS was due, in part, to a decrease in IL-17A production in the CNS. Because *Ifng* and *Il17* were not direct targets of Regnase-1 (*4*, *40*), we further focused on factors promoting T_H1 and T_H17 cell polarization. Luciferase reporter assays revealed that Regnase-1 could directly destabilize a set of T_H1/T_H17 cell–promoting factors such as *Furin* and *Il12rb1* (T_H1), as well as *Nfkbiz* (T_H17; fig. S10E). These data together suggest that Reg1-MO–mediated increase in Regnase-1 expression destabilized the transcripts coding for T cell differentiation factors and altered the production of helper T cell signature cytokines, thus demonstrating the versatility of Reg1-MOs in restricting inflammation through pathways other than direct cytokine suppression.

Next, we investigated whether increasing Regnase-1 expression would affect T_{reg} differentiation or proliferation. Although the majority of naïve CD4$^+$ T cells became FOXP3$^+$ T_{reg} cells at the end point of in vitro differentiation, Reg1-MO treatment did not further increase the percentage of FOXP3$^+$ cells, suggesting that enhancing Regnase-1 abundance did not alter the differentiation of T_{reg} cells in vitro (fig. S10F). This observation confirmed our previous study that T_{reg} development was not impaired in mice under T cell–specific deletion

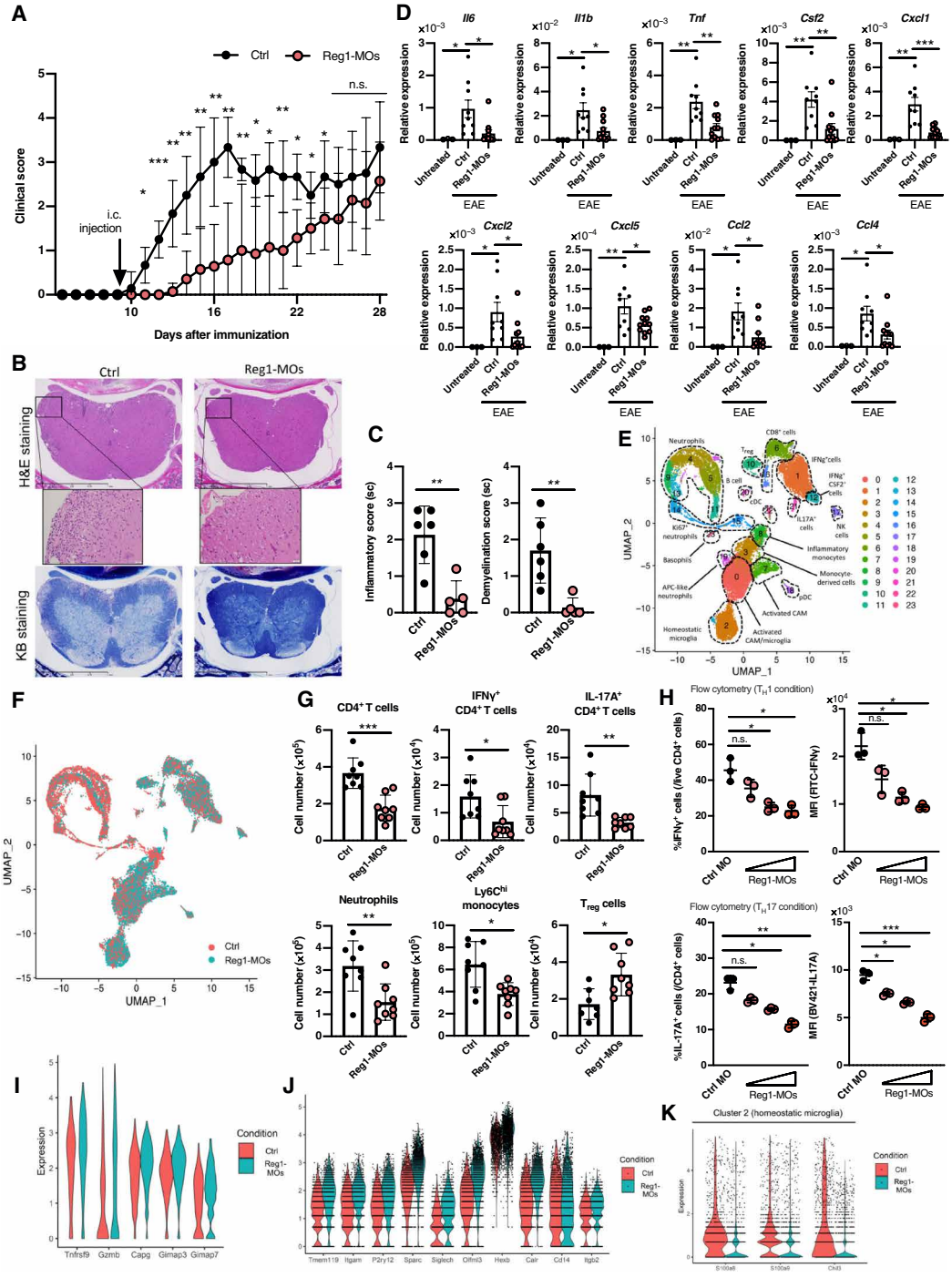

Fig. 5. Increasing Regnase-1 levels in the CNS impaired EAE development. (**A**) EAE clinical scores of B6 mice from the indicated group (Ctrl, $n = 6$; Reg1-MOs, $n = 7$). (**B**) Representative images of spinal cord sections observed by H&E (top) and Kluver-Barrera staining (bottom) from the indicated EAE animals. Scale bars, 250 and 20 μm, respectively. (**C**) Quantitation of inflammation and demyelination scores (Ctrl, $n = 6$; Reg1-MOs, $n = 5$). (**D**) RT-qPCR analyses for the expression level of the indicated genes in the spinal cord of untreated ($n = 3$) and EAE animals of the indicated groups on day 16 (Ctrl, $n = 9$; Reg1-MOs, $n = 11$). Data are representative of two individual experiments. (**E**, **F**, and **I** to **K**) scRNA-seq analysis of spinal cord CD45$^+$ cells derived from EAE mice that received Ctrl or Reg1-MO treatment on 16 days after immunization. (E) A two-dimensional Uniform Manifold Approximation and Projection (UMAP) visualization of spinal cord CD45$^+$ cells isolated from EAE mice receiving the indicated treatment. Each dot represents an individual cell. Dashed lines indicate different cell population. (F) UMAP visualization of CD45$^+$ cells from the Ctrl (red) and Reg1-MO (cyan) groups. The plot shown here was derived by combining two biological replicates. (**G**) Flow cytometry analyses of spinal cord infiltrates harvested at the peak of EAE (d16) from the Ctrl or Reg1-MO group ($n = 8$). Data are representative of two individual experiments. (**H**) Percentage of IFNγ$^+$ cells and IL-17A$^+$ cells and their respective mean fluorescence intensity (MFI) values ($n = 3$ for the indicated condition). Violin plots depicting the transcripts involved in suppression function of T_{regs} (I) homeostatic microglia gene signature (J) and neutrophil chemotaxis molecules (K) between the Ctrl and Reg1-MO groups. *y* axis of the violin plot represents gene expression in log value. Each dot represents a single cell for a specific gene. (A), (C), and (G) show means ± SD, (D) shows means ± SEM. *$P \leq 0.05$; **$P \leq 0.01$; ***$P \leq 0.001$.

of Regnase-1 (*6*). In addition, we found comparable expression of T_{reg} differentiation factors and chemokines important for T_{reg} infiltration to the CNS in the spinal cord of the two groups of EAE mice (fig. S10, G and H) (*41*, *42*). We reasoned that Reg1-MOs do not directly affect the differentiation or infiltration of T_{reg} cells but instead shift the polarization of T cells by suppressing the production/release of cytokines necessary for T_H1 and T_H17 differentiation, such as *Il12p40* and *Il6*, in the CNS (fig. S10I). scRNA-seq revealed that transcripts characteristic of T_{reg} cell–suppressive function, such as *Tnfrsf9*, *Gzmb*, *Capg*, *Gimap7*, and *Gimap3*, were more enriched in the Reg1-MO group (Fig. 5I), suggesting that Reg1-MO treatment not only increased the absolute number of T_{reg} cells but also enhanced their suppressive functions.

Because Reg1-MOs were administered before EAE onset, we hypothesized that CNS-resident immune cells such as microglia would be the major recipients. On the basis of the previous findings (*43*), we observed cluster 2 corresponds to microglia at the homeostatic stage, whereas cluster 0 corresponds to diseased microglia profile in our scRNA-seq data. We observe an increasing trend of expression of homeostatic microglial markers (*44*) in cluster 2 derived from the Reg1-MO group, suggesting that Reg1-MO treatment stalled the microglial transition toward a proinflammatory state (Fig. 5J). The phagocytosis-related genes (*Calr*, *Cd14*, *Itgb2*, and *Itgam*) were more enriched in the homeostatic microglia subsets, implying that microglia from the Reg1-MO–treated group displayed enhanced phagocytotic ability (Fig. 5J). Moreover, Reg1-MO–treated microglia showed reduced expression of *S100a8*, *S100a9*, and *Chil3*, which are important mediators for the chemotaxis and adhesion functions of neutrophils (Fig. 5K) (*45*, *46*). Consistently, we observed lower expression of proinflammatory cytokines (*Il6*, *Il1b*, *Tnf*, and *Csf2*) and chemokine-related transcripts (*Cxcl1*, *Cxcl2*, and *Ccl4*) in spinal cord microglia isolated from the Reg1-MO group (fig. S11, A and B). *Cxcl1* and *Cxcl2*, which play important roles in EAE development (*47*, *48*), are chemokines directly targeted by Regnase-1–mediated mRNA decay (*7*), whereas *Ccl2* and *Ccl4* are crucial chemoattractants of peripheral immune cells to the CNS (*49*–*51*). In addition, Reg1-MO treatment could reduce inflammatory mediator transcripts in BV2 and primary microglia cells upon in vitro stimulation (fig. S11, C and D). Together, Reg1-MO treatment suppressed inflammation in EAE by controlling the immune cell infiltration to the CNS via modification of spinal cord–resident microglia cells through the enhancement of *Regnase-1* expression.

Regnase-1 expression in patients with MS inversely correlated with lesion areas

These results demonstrate that targeting the Regnase-1 autoregulation pathway with Reg1-MOs is an effective strategy to treat inflammatory and autoimmune diseases in mice. To examine whether this strategy is applicable to the treatment of autoimmune diseases in human, we investigated the clinical significance of Regnase-1–mediated regulation in patients with MS by comparing *Regnase-1* mRNA levels in peripheral blood from patients with MS and healthy controls. The patients with MS were 40.3 ± 10.6 (means ± SD) years old, with disease duration of 10.1 ± 9.7 years. Among 22 patients, 21 were treated with disease-modifying drugs: 6 with dimethyl fumarate, 4 with IFN therapy, 4 with fingolimod, 1 with glatiramer acetate, 5 with natalizumab, and 1 with siponimod (table S2). The overall expression of *Regnase-1* in the peripheral blood mononuclear cells (PBMCs) of patients with MS was similar to that of the control subjects, and the mRNA expression of inflammatory cytokines such as *IL6* and *IL1B* were enriched in patients with MS (Fig. 6A). We observed a significant negative correlation between *Regnase-1* mRNA expression and the number of T2-weighted lesions detected by magnetic resonance imaging among 22 patients with MS (*rho* = −0.5288, $P = 0.0114$; Fig. 6B). The T2 lesion burden reflects the degree of brain tissue loss and brain tissue integrity in patients with MS (*52*, *53*), and we hypothesize that lower *Regnase-1* expression may increase the likelihood of inflammation and immune cell activations in patients with MS. Together, these observations highlight the possible application of Regnase-1–targeting MOs toward the treatment of autoimmune diseases like MS. Consistently, MOs against human *Regnase-1* SL structures not only increased the *Regnase-1* expression in human monocytic cells (U937 and THP-1) and in peripheral $CD14^+$ monocytes isolated from healthy controls, but also blunted their proinflammatory gene expression profiles upon LPS stimulation (Fig. 6, C to E). Overall, these results demonstrated that enhancing *Regnase-1* expression tipped the balance toward an anti-inflammatory state in human cells (fig. S12).

DISCUSSION

In this study, we developed a potential therapeutic strategy against inflammation by targeting Regnase-1. Comprehensive screening of the mouse *Regnase-1* 3′UTR allowed the identification of two independent SL structures (SL1 and SL2), which were essential for the self-degradation of *Regnase-1* mRNA. Disrupting the two SL structures simultaneously by Reg1-MOs abolished binding of Regnase-1 toward its mRNA and blocked its autoregulation. Reg1-MO–dependent augmentation of Regnase-1 availability effectively destabilized a set of inflammatory mRNAs in BMDMs upon LPS stimulation. Transcriptomic analysis revealed that Reg1-MO treatment had undetectable immunostimulatory activity toward innate nucleic acid sensors.

The use of Reg1-MOs is effective in alleviating inflammation in several disease models. In the LPS-injured lung, Reg1-MO treatment reduced the production of proinflammatory and chemokine-related transcripts in alveolar cells, especially AMs, thereby decreasing the neutrophil infiltration to lung and improving pulmonary congestion. In addition, enhancing *Regnase-1* expression was therapeutically effective in attenuating lung fibrosis by actively reducing both inflammatory and profibrotic factors in alveolar cells. Further investigation is needed for other immune cells such as ILC2s or nonhematopoietic cells, including epithelial cells and fibroblasts, which play important roles in the pathogenesis of pulmonary fibrosis (*54*, *55*). Last, intracranial administration of Reg1-MOs to EAE mice impaired disease development. Flow cytometry analysis and scRNA-seq results revealed that the effect of Reg1-MOs was associated with a decrease in CNS-infiltrating neutrophils. Because neutrophils have highly proinflammatory function and destructive capacity (*48*, *56*, *57*), reducing neutrophil infiltration to the CNS prevented further release of cytokines and reactivation of the infiltrated T cells, which helped to preserve the integrity of the blood-brain barrier (*48*). We reasoned that Reg1-MOs restricted neutrophil infiltration to the CNS by limiting the production of chemokines and cytokines from CNS-resident microglia and T cells. In vitro experiments culturing microglia cells or $CD4^+$ T cells with Reg1-MOs revealed that increasing Regnase-1 abundance in these two cell types altered their secretion of inflammatory molecules and their differentiation potentials, respectively. *Regnase-1* expression also negatively correlated with disease severity

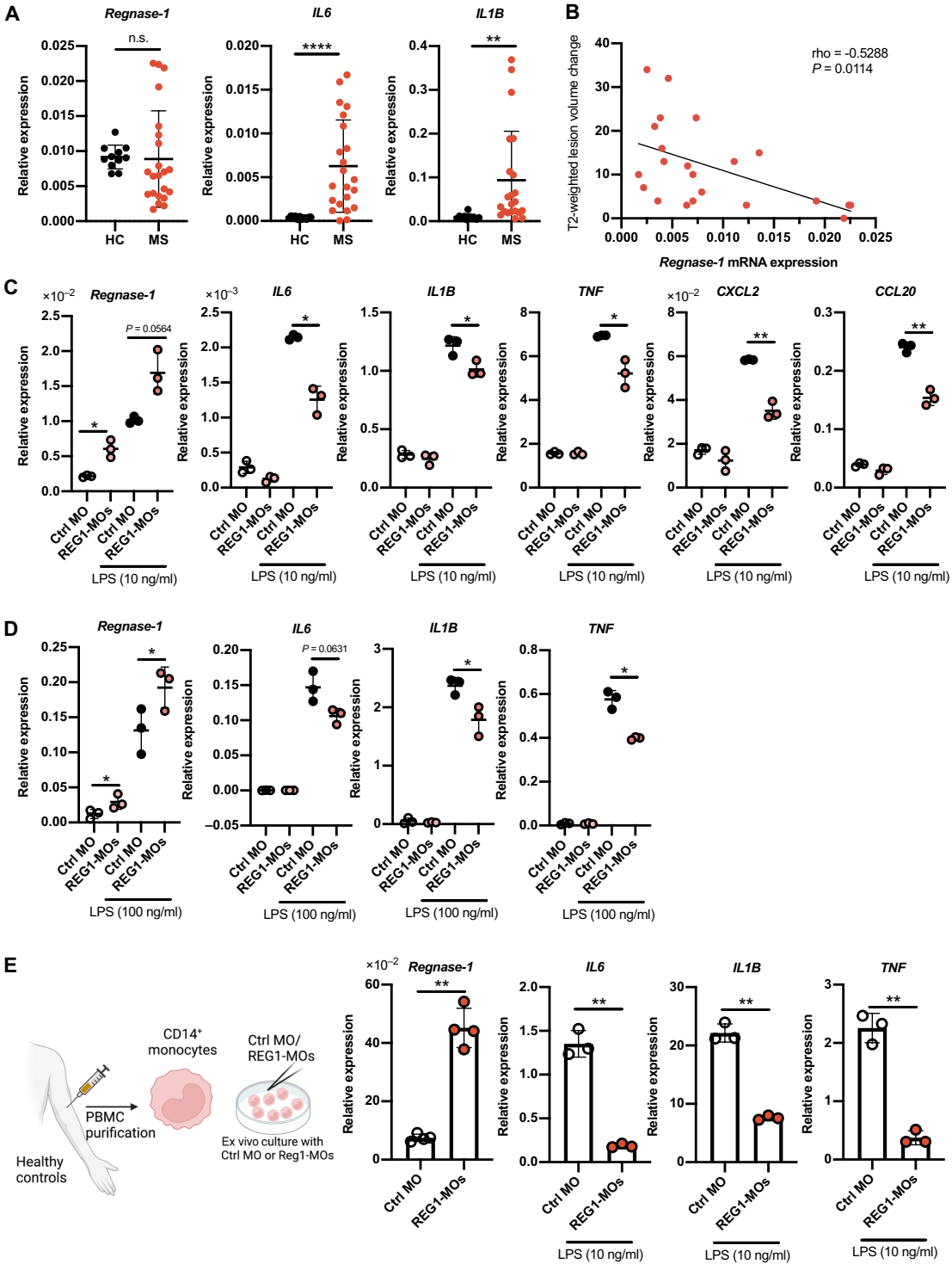

Fig. 6. *Regnase-1* expression negatively correlates with MS disease severity. (**A**) RT-qPCR analyses for the expression level of *Regnase-1*, *IL6*, and *IL1B* in PBMCs derived from healthy controls (HC; $n = 11$) and patients with multiple sclerosis (MS; $n = 22$). (**B**) Correlation between *Regnase-1* mRNA expression (*x* axis) and T2-weighted lesion volume change (*y* axis). Spearman's rank correlation was used for the analysis (rho = Spearman's rank correlation coefficient; $P < 0.05$ = significant). RT-qPCR analyses for the expressions of the indicated genes in PMA-differentiated (**C**) U937cells and (**D**) THP-1 cells transfected with Ctrl MO or REG1-MOs, followed by stimulation with LPS ($n = 3$ per group). (**E**) Left: Outline of the ex vivo culture of HC-derived peripheral $CD14^+$ monocytes with Ctrl MO or REG1-MOs, before being stimulated with LPS for 4 hours. Right: RT-qPCR analyses for the expression of human *Regnase-1* and proinflammatory cytokines upon LPS stimulation. (A) shows means ± SEM, (C) to (E) shows means ± SD. $^*P \le 0.05$; $^{**}P \le 0.01$; $^{****}P \le 0.0001$.

in patients with MS, highlighting the fact that manipulation of Regnase-1 availability by MOs could be beneficial in treating human inflammatory and autoimmune diseases.

Biological therapies that target proteins involved the inflammatory processes are being evaluated in clinical trials to treat inflammatory and autoimmune diseases and are being used in addition to immunosuppressants. Neutralizing antibodies targeting cytokines such as TNF and IL-6, or their associated signaling pathways have been widely used as anti-inflammatory therapies to modulate immune response (*58*, *59*). However, a percentage of patients with autoimmune diseases are resistant to the blockade of a single cytokine, suggesting that simultaneous suppression of the production of multiple proinflammatory transcripts could be a potentially better strategy. Because the target of Reg1-MOs is distinct from the current available therapeutics, Reg1-MO therapy may potentially be used in combination with other drug therapeutics to modulate the inflammatory responses in diseases in which Regnase-1 deficiency was shown to worsen disease pathogenesis (*9*, *40*, *60*, *61*). However, considering the finding that Regnase-1 depletion enhanced cytotoxic T cell function within the tumor microenvironment (*14*), approaches to specifically attenuate Regnase-1 expression also warrant attention. For example, usage of small interfering RNA–based gene knockdown and CRISPR-Cas9 gene-editing technology is a potential strategy to reduce or delete Regnase-1 expression in a cell-specific manner. In addition, inhibition of SMG1 kinase abrogated Regnase-1–mediated mRNA decay by disrupting the association between Regnase-1 and the UPF1 helicase (*8*), thus highlighting the therapeutic potential of SMG1 inhibitor in potentiating the activation of innate immune cells.

This study has several limitations. First, most of our studies rely on the use of mouse and human cell lines, as well as mouse models, for the examination of the anti-inflammatory aspects of Reg1-MOs, and we and others have not yet demonstrated the efficacy of REG1-MOs in human clinical studies. In addition, we used MOs to target Regnase-1 in this study considering their potential for clinical utility, but further investigation is required to optimize the ASO modality, delivery system, and delivery routes to maximize the therapeutic efficacy. Autoimmune diseases like rheumatoid arthritis and systemic lupus erythematosus are characterized by the development of systemic lesions. Thus, studies are required to develop a strategy for the delivery of MOs systematically for therapeutic intervention. Although we have demonstrated the preliminary safety in targeting the inflammatory response by Reg1-MOs, it is necessary to conduct further toxicological and pharmacological studies before clinical application in humans.

MATERIALS AND METHODS

Study design

The goal of this study is to develop a strategy to restrict inflammatory diseases by manipulating Regnase-1 expression through the usage of morpholino-based ASOs. We found that blocking the Regnase-1 self-regulation pathway not only increased Regnase-1 abundance but also counteracted the adverse effects of inflammation. We evaluated the efficacy of Reg1-targeting MOs in vivo with the use of acute and chronic inflammatory disease models including LPS-induced ARDS and bleomycin-induced lung fibrosis models, and an autoimmune mouse model, EAE. Last, human PBMC samples from patients with MS were analyzed for evaluating the association between Regnase-1 expression and clinical significance.

All in vitro and in vivo experiments were replicated at least twice and were performed at least in biological triplicates. Animals were randomized to experimental groups, and no mice were excluded from the experiment. Gene expression and flow cytometry analyses were performed unblinded. All animal experiments were performed in accordance with the National Institutes of Health *Guide for the Care and Use of Laboratory Animals* and approved by the Animal Research Committee, Graduate School of Medicine, Kyoto University (permit number 120002). Age- and gender-matched littermates of the same strain were used in each experiment. Anonymous patient PBMC samples were obtained from the Graduate School of Medicine, Osaka University, Japan (permit number 11298-22).

Antisense MO and transfection

The sequence for mouse *Regnase-1* MO1 and MO2 (targeting 3′end of the stem) are CTTAAATGACAGAGATACAATGT and CCTCAGAGAGCAGGCACATG, and those targeting the 5′end of mRegnase-1 SL-1 and SL-2 and outside SL have the following sequences: AATGTGTATCAACAGGGTGAT, ATGGTGCCTAACTAGCCGGT, and GGCAGCGTCTCCTTAAATGAC, respectively, and were synthesized as bare MO, 3′-carboxyfluorescein–tagged MO, or Vivo-MO (Gene Tools LLC, USA). The sequences for human *Regnase-1* MO1 and MO2 are CTTAAACTACAGAGATACAATGT and ACGGTGCCCAACTAGCCAG, respectively, and were synthesized as bare MO. MO with the sequence CCTCTTACCTCAGTTAGAATTTATA was used as a standard control for all experiments (bare MO or Vivo-MO). MOs were dissolved in sterile water for in vitro experiments (stock concentration, 0.5 mM) and in sterile saline solution for in vivo experiments (5 μg/μl). In vitro delivery of MOs was achieved by Endoporter (GeneTools).

Mice and mouse model establishment

Female C57BL/6J (B6) mice were purchased from CLEA Japan Inc. (Tokyo, Japan). All experiments were conducted on 8- to 12-week-old mice. *Regnase-1*$^{-/-}$ mice have been described previously (*4*). For the induction of acute lung injury and pulmonary fibrosis, C57BL/6 mice were intratracheally administrated with *Escherichia coli*–derived LPS (10 μg; InvivoGen) or bleomycin sulfate (0.021 U per mouse; LKT Labs). Active EAE was induced in C57BL/6 mice by subcutaneous injection of 100 μg of MOG peptide (Anaspec) emulsified in complete Freund's adjuvant supplemented with killed *Mycobacterium tuberculosis* (4 mg/ml; Chondrex) on day 0. Mice were injected intraperitoneally with 200 ng of pertussis toxin (List Biological laboratories, INC) on days 0 and 2 unless otherwise specified. Detailed treatment protocol is described in the Supplementary Text.

Biological sample collection

Isolation of single-cell suspension from the lung tissue was performed as described previously (*13*). BAL fluid was collected by four consecutive instillations of 1.0 ml of phosphate-buffered saline (PBS). For the isolation of CNS cells, mice were perfused with ice-cold PBS via the left ventricle. CNS tissues were cut into small pieces and digested in Hanks' balanced salt solution–positive buffer (Nacalai Tesque) supplemented with 2% fetal bovine serum (FBS), penicillin-streptomycin, Hepes, and collagenase D (160 U; Roche Applied Science) for 35 min at 37°C. The CNS single-cell suspension was obtained by passing the material through an 18-gauge needle, followed by filtration through a cell strainer. Cell pellet was resuspended in 38% Percoll,

and the myelin fraction was separated from mononuclear cells by density centrifugation. Details are described in the Supplementary Text.

Luciferase reporter assay

HeLa cells were transfected with the Firefly luciferase reporter plasmid (Promega) containing the 3′UTR of indicated genes, with or without Regnase-1 expression plasmids, by Lipofectamine 2000 or Lipofectamine LTX (Invitrogen), according to the manufacturer's instructions. The gene encoding *Renilla* luciferase was transfected simultaneously as internal control. Cells were lysed 16 to 24 hours after transfection, and the luciferase activity in the lysates was measured using the Dual-luciferase Reporter Assay system (Promega).

Histological examination

For in vivo lung experiments, lungs were fixed with Mildform 10 N and embedded in paraffin blocks. Sections of 4 μm were stained with hematoxylin and eosin (H&E), Verhoeff Van Gieson (EVG), or Azan-Mallory dyes. For the isolation of spinal cord, EAE mice were perfused by cardiac puncture of the left ventricle with 37% formalin. The entire spinal column was removed and fixed with formalin for 48 hours as previously described (*62*), before subjected to tissue preparation and sectioning. Sections of 5-μm thickness were subjected to H&E and Kluver-Barrera staining for the evaluation of inflammatory cell infiltration and demyelination, respectively (details can be found in the Supplementary Materials).

Immunoblotting

Whole-cell extracts were prepared in SDS sample buffer containing 20 mM tris-HCl (pH 8.0), 150 mM NaCl, 10 mM EDTA, 1% NP-40, 0.1% SDS, 1% sodium deoxycholate, 5% β-mercaptoethanol, 10% glycerol and bromophenol blue, and 1 tablet of cOmplete Mini Protease Inhibitor Cocktail without EDTA (Roche Applied Science). Samples were boiled for 5 min at 95°C and analyzed using the following antibodies: polyclonal rabbit anti-mouse/human Regnase-1 (*5*) and anti-β-actin–horseradish peroxidase (HRP) (sc-47778; Santa Cruz Biotechnology) and rabbit immunoglobulin G (IgG) HRP-linked F(ab')2 fragment (NA9340, cytiva). Luminescence was detected with a luminescent image analyzer (ImageQuant LAS 4000, GE Healthcare).

RNA immunoprecipitation–RT-qPCR

HeLa cells were lysed with RNA immunoprecipitation lysis buffer [20 mM tris-HCl (pH 7.4), 150 mM NaCl, 0.5% NP-40, cOmplete Mini Protease Inhibitor Cocktail without EDTA, and 50 μl of RNaseOUT (Invitrogen)]. Lysates were precleared with prewashed Protein G Dynabeads (Invitrogen) at 4°C with rotation for 1 hour. Anti-FLAG antibodies (F3165, Sigma-Aldrich) were conjugated to protein G Dynabeads at 4°C with rotation for 1 hour, before being incubated with the precleared lysates at 4°C for 3 hours. After being washed twice with RNA immunoprecipitation lysis buffer, the RNA and protein from the beads were respectively eluted using TRIzol (Invitrogen) or SDS sample buffer (see above).

RNA isolation, reverse transcription, and qPCR analysis

Total RNA was isolated by TRIzol or Isogen II (Nippongene) according to the manufacturer's instructions. cDNA was reversely transcribed from total RNA samples using ReverTraAce with gDNA remover (TOYOBO) according to the manufacturer's instructions. The synthesized cDNAs were amplified using Thunderbird SYBR qPCR Mix (TOYOBO), and the relative RNA expression levels were measured by SYBR Green Real-Time PCR in StepOnePlus system (Applied Biosystems). Results were normalized to the expression levels of the housekeeping *Gapdh* or *GAPDH* mRNA. Primer sequences are listed in table S3.

Patient information

Detailed information about the patients with MS is described in Results. Samples of peripheral blood were taken from different patients at different time points. All the patients with MS fulfilled the McDonald criteria for MS (*63*). This study has been approved by the Ethics Committee, Osaka University Hospital, Osaka, Japan (permit number 11298-22). Written informed consents were obtained from all participants.

Flow cytometry

Cells were washed in MACS buffer (PBS supplemented with 2% bovine serum albumin and 500 mM EDTA), incubated with specific sets of antibodies for 15 min, and washed twice with MACS buffer before flow cytometry analysis. For intracellular staining, cells were permeabilized with Foxp3 staining buffer set (eBioscience). Antibody information is described in the Supplementary Materials.

In vitro CD4$^+$ T cell differentiation

Naïve CD4$^+$ T cells were isolated from the spleen and lymph nodes from naïve C57BL/6 mice by fluorescence-activated cell sorting and were cultured in RPMI (T_H0, T_H1, or induced T_{reg} condition) or IMDM (T_H17 condition) medium. For T cell polarization, cells were seeded in plates precoated with goat anti-hamster IgG (1:20) and were activated with soluble anti-CD3, anti-CD28 in the presence of the following cytokines: T_H0 condition (IL-2), T_H1 condition (IL-2, IL-12, and anti-IL-4), T_H17 condition (IL-6, IL-1β, IL-23, anti-IL-4, and anti-IFNγ), and induced T_{reg} condition [IL-2, transforming growth factor–β (TGF-β), anti-IL-4, and anti-IFNγ], in the presence of Ctrl MO or Reg1-MOs (5, 10, and 20 μM) and endoporter. Cells were restimulated with phorbol 12-myristate 13-acetate (PMA)/ionmycin in the presence of Golgi Plug before analysis for cytokines (detailed antibody information and culture condition is provided in the Supplementary Materials).

RNA sequencing

BMDMs were treated with Ctrl MO or Reg1-MOs and stimulated with LPS (10 ng/ml) for 4 hours, and the RNA was isolated with TRIzol reagent and purified using RNA clean & Concentrator-5 (Zymo Research). The cDNA libraries were prepared by NEBNext Ultra II Directional RNA Library Prep Kit (Illumina) according to the manufacturer's instructions, and the samples were sequenced on a NextSeq500 (Illumina, 75 cycles). Acquired data were analyzed using Galaxy (see the Supplementary Materials).

Single-cell RNA sequencing

At day 16 after EAE immunization, spinal cord was resected and digested, and CD45$^+$ immune cells were isolated by cell sorting with BD FACSAria III and resuspended with 1× PBS supplemented with 2% FBS. Cell counts were about 7×10^5 cells per milliliter, and viability was above 90%. Single cells were partitioned using a Chromium Controller (10x Genomics), and gene expression sequencing libraries were generated using Chromium Single Cell 3' Library & Gel Bead kit v3 (10x Genomics), following the standard manufacturer's protocol.

Statistical analysis

Statistical analyses were conducted using Prism8 (GraphPad, La Jolla, CA, USA) or Excel for Office 365. Statistical significance was estimated with an unpaired two-tailed Student's *t* test (for two groups), one-way analysis of variance (ANOVA) followed by Brown-Forsythe and Welch ANOVA's multiple-comparison tests to analyze differences among three or more groups, or by two-way ANOVA followed by Sidak's multiple-comparison test to compare multiple factors. Data are represented as means with standard deviations (±SD), unless otherwise mentioned. Spearman's rank correlation test was used for the analysis of clinical samples. Statistical significance was defined as $*P \leq 0.05$, $**P \leq 0.01$, $***P \leq 0.001$, and $****P \leq 0.0001$.

SUPPLEMENTARY MATERIALS

www.science.org/doi/10.1126/scitranslmed.abo2137
Materials and Methods
Figs. S1 to S12
Tables S1 to S3
Data files S1 to S4
MDAR Reproducibility Checklist
References (*64*–*73*)

View/request a protocol for this paper from *Bio-protocol*.

REFERENCES AND NOTES

1. P. Anderson, Post-transcriptional control of cytokine production. *Nat. Immunol.* **9**, 353–359 (2008).
2. T. Glisovic, J. L. Bachorik, J. Yong, G. Dreyfuss, RNA-binding proteins and post-transcriptional gene regulation. *FEBS Lett.* **582**, 1977–1986 (2008).
3. S. Carpenter, E. P. Ricci, B. C. Mercier, M. J. Moore, K. A. Fitzgerald, Post-transcriptional regulation of gene expression in innate immunity. *Nat. Rev. Immunol.* **14**, 361–376 (2014).
4. K. Matsushita, O. Takeuchi, D. M. Standley, Y. Kumagai, T. Kawagoe, T. Miyake, T. Satoh, H. Kato, T. Tsujimura, H. Nakamura, S. Akira, Zc3h12a is an RNase essential for controlling immune responses by regulating mRNA decay. *Nature* **458**, 1185–1190 (2009).
5. H. Iwasaki, O. Takeuchi, S. Teraguchi, K. Matsushita, T. Uehata, K. Kuniyoshi, T. Satoh, T. Saitoh, M. Matsushita, D. M. Standley, S. Akira, The IκB kinase complex regulates the stability of cytokine-encoding mRNA induced by TLR-IL-1R by controlling degradation of regnase-1. *Nat. Immunol.* **12**, 1167–1175 (2011).
6. T. Uehata, H. Iwasaki, A. Vandenbon, K. Matsushita, E. Hernandez-Cuellar, K. Kuniyoshi, T. Satoh, T. Mino, Y. Suzuki, D. M. Standley, T. Tsujimura, H. Rakugi, Y. Isaka, O. Takeuchi, S. Akira, Malt1-induced cleavage of regnase-1 in CD4(+) helper T cells regulates immune activation. *Cell* **153**, 1036–1049 (2013).
7. T. Mino, Y. Murakawa, A. Fukao, A. Vandenbon, H. H. Wessels, D. Ori, T. Uehata, S. Tartey, S. Akira, Y. Suzuki, C. G. Vinuesa, U. Ohler, D. M. Standley, M. Landthaler, T. Fujiwara, O. Takeuchi, Regnase-1 and roquin regulate a common element in inflammatory mRNAs by spatiotemporally distinct mechanisms. *Cell* **161**, 1058–1073 (2015).
8. T. Mino, N. Iwai, M. Endo, K. Inoue, K. Akaki, F. Hia, T. Uehata, T. Emura, K. Hidaka, Y. Suzuki, D. M. Standley, M. Okada-Hatakeyama, S. Ohno, H. Sugiyama, A. Yamashita, O. Takeuchi, Translation-dependent unwinding of stem-loops by UPF1 licenses Regnase-1 to degrade inflammatory mRNAs. *Nucleic Acids Res.* **47**, 8838–8859 (2019).
9. X. Cui, T. Mino, M. Yoshinaga, Y. Nakatsuka, F. Hia, D. Yamasoba, T. Tsujimura, K. Tomonaga, Y. Suzuki, T. Uehata, O. Takeuchi, Regnase-1 and roquin nonredundantly regulate Th1 differentiation causing cardiac inflammation and fibrosis. *J. Immunol.* **199**, 4066–4077 (2017).
10. Y. Nakatsuka, A. Vandenbon, T. Mino, M. Yoshinaga, T. Uehata, X. Cui, A. Sato, T. Tsujimura, Y. Suzuki, A. Sato, T. Handa, K. Chin, T. Sawa, T. Hirai, O. Takeuchi, Pulmonary regnase-1 orchestrates the interplay of epithelium and adaptive immune systems to protect against pneumonia. *Mucosal Immunol.* **11**, 1203–1218 (2018).
11. K. Nanki, M. Fujii, M. Shimokawa, M. Matano, S. Nishikori, S. Date, A. Takano, K. Toshimitsu, Y. Ohta, S. Takahashi, S. Sugimoto, K. Ishimaru, K. Kawasaki, Y. Nagai, R. Ishii, K. Yoshida, N. Sasaki, T. Hibi, S. Ishihara, T. Kanai, T. Sato, Somatic inflammatory gene mutations in human ulcerative colitis epithelium. *Nature* **577**, 254–259 (2020).
12. N. Kakiuchi, K. Yoshida, M. Uchino, T. Kihara, K. Akaki, Y. Inoue, K. Kawada, S. Nagayama, A. Yokoyama, S. Yamamoto, M. Matsuura, T. Horimatsu, T. Hirano, N. Goto, Y. Takeuchi, Y. Ochi, Y. Shiozawa, Y. Kogure, Y. Watatani, Y. Fujii, S. K. Kim, A. Kon, K. Kataoka, T. Yoshizato, M. M. Nakagawa, A. Yoda, Y. Nanya, H. Makishima, Y. Shiraishi, K. Chiba, H. Tanaka, M. Sanada, E. Sugihara, T. A. Sato, T. Maruyama, H. Miyoshi, M. M. Taketo, J. Oishi, R. Inagaki, Y. Ueda, S. Okamoto, H. Okajima, Y. Sakai, T. Sakurai, H. Haga, S. Hirota, H. Ikeuchi, H. Nakase, H. Marusawa, T. Chiba, O. Takeuchi, S. Miyano, H. Seno, S. Ogawa, Frequent mutations that converge on the NFKBIZ pathway in ulcerative colitis. *Nature* **577**, 260–265 (2020).
13. Y. Nakatsuka, A. Yaku, T. Handa, A. Vandenbon, Y. Hikichi, Y. Motomura, A. Sato, M. Yoshinaga, K. Tanizawa, K. Watanabe, T. Hirai, K. Chin, Y. Suzuki, T. Uehata, T. Mino, T. Tsujimura, K. Moro, O. Takeuchi, Profibrotic function of pulmonary group 2 innate lymphoid cells is controlled by regnase-1. *Eur. Respir. J.* **57**, 2000018 (2021).
14. J. Wei, L. Long, W. Zheng, Y. Dhungana, S. A. Lim, C. Guy, Y. Wang, Y. D. Wang, C. Qian, B. Xu, A. Kc, J. Saravia, H. Huang, J. Yu, J. G. Doench, T. L. Geiger, H. Chi, Targeting REGNASE-1 programs long-lived effector T cells for cancer therapy. *Nature* **576**, 471–476 (2019).
15. N. Delihas, S. E. Rokita, P. Zheng, Natural antisense RNA/target RNA interactions: Possible models for antisense oligonucleotide drug design. *Nat. Biotechnol.* **15**, 751–753 (1997).
16. W. Lima, H. Wu, S. T. Crooke, The RNase H mechanism, in *Antisense Drug Technology: Principles, Strategies, and Applications* (CRC Press, ed. Second Edition, 2007), pp. 65–92.
17. D. A. Melton, Injected anti-sense RNAs specifically block messenger RNA translation in vivo. *Proc. Natl. Acad. Sci. U.S.A.* **82**, 144–148 (1985).
18. D. Hodges, S. T. Crooke, Inhibition of splicing of wild-type and mutated luciferase-adenovirus pre-mRNAs by antisense oligonucleotides. *Mol. Pharmacol.* **48**, 905–918 (1995).
19. R. S. Finkel, E. Mercuri, B. T. Darras, A. M. Connolly, N. L. Kuntz, J. Kirschner, C. A. Chiriboga, K. Saito, L. Servais, E. Tizzano, H. Topaloglu, M. Tulinius, J. Montes, A. M. Glanzman, K. Bishop, Z. J. Zhong, S. Gheuens, C. F. Bennett, E. Schneider, W. Farwell, D. C. De Vivo, Nusinersen versus sham control in infantile-onset spinal muscular atrophy. *N. Engl. J. Med.* **377**, 1723–1732 (2017).
20. J. S. Charleston, F. J. Schnell, J. Dworzak, C. Donoghue, S. Lewis, L. Chen, G. D. Young, A. J. Milici, J. Voss, U. DeAlwis, B. Wentworth, L. R. Rodino-Klapac, Z. Sahenk, D. Frank, J. R. Mendell, Eteplirsen treatment for Duchenne muscular dystrophy: Exon skipping and dystrophin production. *Neurology* **90**, e2146–e2154 (2018).
21. U. A. Ørom, S. Kauppinen, A. H. Lund, LNA-modified oligonucleotides mediate specific inhibition of microRNA function. *Gene* **372**, 137–141 (2006).
22. S. T. Crooke, X. H. Liang, R. M. Crooke, B. F. Baker, R. S. Geary, Antisense drug discovery and development technology considered in a pharmacological context. *Biochem. Pharmacol.* **189**, 114196 (2021).
23. T. C. Roberts, R. Langer, M. J. A. Wood, Advances in oligonucleotide drug delivery. *Nat. Rev. Drug Discov.* **19**, 673–694 (2020).
24. S. T. Crooke, B. F. Baker, R. M. Crooke, X. H. Liang, Antisense technology: An overview and prospectus. *Nat. Rev. Drug Discov.* **20**, 427–453 (2021).
25. S. M. García-Mauriño, F. Rivero-Rodríguez, A. Velázquez-Cruz, M. Hernández-Vellisca, A. Díaz-Quintana, M. A. De la Rosa, I. Díaz-Moreno, RNA binding protein regulation and cross-talk in the control of AU-rich mRNA fate. *Front. Mol. Biosci.* **4**, (2017).
26. P. A. Morcos, Y. Li, S. Jiang, Vivo-Morpholinos: A non-peptide transporter delivers Morpholinos into a wide array of mouse tissues. *Biotechniques* **45**, 613–614 (2008).
27. L. K. Johnston, C. R. Rims, S. E. Gill, J. K. McGuire, A. M. Manicone, Pulmonary macrophage subpopulations in the induction and resolution of acute lung injury. *Am. J. Respir. Cell Mol. Biol.* **47**, 417–426 (2012).
28. A. Sica, A. Mantovani, Macrophage plasticity and polarization: In vivo veritas. *J. Clin. Investig.* **122**, 787–795 (2012).
29. P. A. Ward, G. W. Hunninghake, Lung inflammation and fibrosis. *Am. J. Respir. Critical Care Med.* **157**, S123–S129 (1998).
30. A. H. Gifford, M. Matsuoka, L. Y. Ghoda, R. J. Homer, R. I. Enelow, Chronic inflammation and lung fibrosis: Pleotropic syndromes but limited distinct phenotypes. *Mucosal Immunol.* **5**, 480–484 (2012).
31. K. Shenderov, S. L. Collins, J. D. Powell, M. R. Horton, Immune dysregulation as a driver of idiopathic pulmonary fibrosis. *J. Clin. Investig.* **131**, e143226 (2021).
32. N. Khalil, O. Bereznay, M. Sporn, A. H. Greenberg, Macrophage production of transforming growth factor beta and fibroblast collagen synthesis in chronic pulmonary inflammation. *J. Exp. Med.* **170**, 727–737 (1989).
33. T. A. Wynn, K. M. Vannella, Macrophages in tissue repair, regeneration, and fibrosis. *Immunity* **44**, 450–462 (2016).
34. M. Sospedra, R. Martin, Immunology of multiple sclerosis. *Semin. Neurol.* **36**, 115–127 (2016).
35. A. V. Garg, N. Amatya, K. Chen, J. A. Cruz, P. Grover, N. Whibley, H. R. Conti, G. H. Mir, T. Sirakova, E. C. Childs, T. E. Smithgall, P. S. Biswas, J. K. Kolls, M. J. McGeachy, P. E. Kolattukudy, S. L. Gaffen, MCPIP1 endoribonuclease activity negatively regulates interleukin-17-mediated signaling and inflammation. *Immunity* **43**, 475–487 (2015).
36. A. Ben-Nun, H. Wekerle, I. R. Cohen, The rapid isolation of clonable antigen-specific T lymphocyte lines capable of mediating autoimmune encephalomyelitis. *Eur. J. Immunol.* **11**, 195–199 (1981).
37. D. G. Ando, J. Clayton, D. Kono, J. L. Urban, E. E. Sercarz, Encephalitogenic T cells in the B10.PL model of experimental allergic encephalomyelitis (EAE) are of the Th-1 lymphokine subtype. *Cell. Immunol.* **124**, 132–143 (1989).
38. C. L. Langrish, Y. Chen, W. M. Blumenschein, J. Mattson, B. Basham, J. D. Sedgwick, T. McClanahan, R. A. Kastelein, D. J. Cua, IL-23 drives a pathogenic T cell population that induces autoimmune inflammation. *J. Exp. Med.* **201**, 233–240 (2005).

39. M. A. Kroenke, T. J. Carlson, A. V. Andjelkovic, B. M. Segal, IL-12- and IL-23-modulated T cells induce distinct types of EAE based on histology, CNS chemokine profile, and response to cytokine inhibition. *J. Exp. Med.* **205**, 1535–1541 (2008).
40. L. Monin, J. E. Gudjonsson, E. E. Childs, N. Amatya, X. Xing, A. H. Verma, B. M. Coleman, A. V. Garg, M. Killeen, A. Mathers, N. L. Ward, S. L. Gaffen, MCPIP1/Regnase-1 restricts IL-17A- and IL-17C-dependent skin inflammation. *J. Immunol.* **198**, 767–775 (2017).
41. T. Yamazaki, X. O. Yang, Y. Chung, A. Fukunaga, R. Nurieva, B. Pappu, N. Martin-Orozco, H. S. Kang, L. Ma, A. D. Panopoulos, S. Craig, S. S. Watowich, A. M. Jetten, Q. Tian, C. Dong, CCR6 regulates the migration of inflammatory and regulatory T cells. *J. Immunol.* **181**, 8391–8401 (2008).
42. M. Ito, K. Komai, S. Mise-Omata, M. Iizuka-Koga, Y. Noguchi, T. Kondo, R. Sakai, K. Matsuo, T. Nakayama, O. Yoshie, H. Nakatsukasa, S. Chikuma, T. Shichita, A. Yoshimura, Brain regulatory T cells suppress astrogliosis and potentiate neurological recovery. *Nature* **565**, 246–250 (2019).
43. M. J. C. Jordão, R. Sankowski, S. M. Brendecke, S. G. Locatelli, Y. H. Tai, T. L. Tay, E. Schramm, S. Armbruster, N. Hagemeyer, O. Groß, D. Mai, Ö. Çiçek, T. Falk, M. Kerschensteiner, D. Grün, M. Prinz, Single-cell profiling identifies myeloid cell subsets with distinct fates during neuroinflammation. *Science* **363**, eaat7554 (2019).
44. S. E. Hickman, N. D. Kingery, T. K. Ohsumi, M. L. Borowsky, L. C. Wang, T. K. Means, J. El Khoury, The microglial sensome revealed by direct RNA sequencing. *Nature Neurosci.* **16**, 1896–1905 (2013).
45. C. Ryckman, K. Vandal, P. Rouleau, M. Talbot, P. A. Tessier, Proinflammatory activities of S100: Proteins S100A8, S100A9, and S100A8/A9 induce neutrophil chemotaxis and adhesion. *J. Immunol.* **170**, 3233–3242 (2003).
46. T. E. Sutherland, N. Logan, D. Rückerl, A. A. Humbles, S. M. Allan, V. Papayannopoulos, B. Stockinger, R. M. Maizels, J. E. Allen, Chitinase-like proteins promote IL-17-mediated neutrophilia in a tradeoff between nematode killing and host damage. *Nature Immunol.* **15**, 1116–1125 (2014).
47. T. Carlson, M. Kroenke, P. Rao, T. E. Lane, B. Segal, The Th17-ELR$^+$ CXC chemokine pathway is essential for the development of central nervous system autoimmune disease. *J. Exp. Med.* **205**, 811–823 (2008).
48. J. M. Rumble, A. K. Huber, G. Krishnamoorthy, A. Srinivasan, D. A. Giles, X. Zhang, L. Wang, B. M. Segal, Neutrophil-related factors as biomarkers in EAE and MS. *J. Exp. Med.* **212**, 23–35 (2015).
49. K. Kennedy, R. Strieter, S. Kunkel, N. Lukacs, W. Karpus, Acute and relapsing experimental autoimmune encephalomyelitis are regulated by differential expression of the CC chemokines macrophage inflammatory protein-1alpha and monocyte chemotactic protein-1. *J. Meuroimmunol.* **92**, 98–108 (1998).
50. S. Youssef, G. Wildbaum, N. Karin, Prevention of experimental autoimmune encephalomyelitis by MIP-1alpha and MCP-1 naked DNA vaccines. *J. Autoimmun.* **13**, 21–29 (1999).
51. M. Soleimani, A. Soleymani, N. Seyyedirad, Elevated CSF concentration of CCL3 and CCL4 in relapsing remitting multiple sclerosis patients. *J. Immunoassay Immunochem.* **40**, 378–385 (2019).
52. R. A. Rudick, J. C. Lee, J. Simon, E. Fisher, Significance of T2 lesions in multiple sclerosis: A 13-year longitudinal study. *Ann. Neurol.* **60**, 236–242 (2006).
53. J. P. Mostert, M. W. Koch, C. Steen, D. J. Heersema, J. C. De Groot, J. De Keyser, T2 lesions and rate of progression of disability in multiple sclerosis. *Eur. J. Neurol.* **17**, 1471–1475 (2010).
54. D. C. Rockey, P. D. Bell, J. A. Hill, Fibrosis--A common pathway to organ injury and failure. *N. Engl. J. Med.* **372**, 1138–1149 (2015).
55. G. Bagnato, S. Harari, Cellular interactions in the pathogenesis of interstitial lung diseases. *Eur. Respir. Rev.* **24**, 102–114 (2015).
56. B. Aubé, S. A. Lévesque, A. Paré, É. Chamma, H. Kébir, R. Gorina, M. A. Lécuyer, J. I. Alvarez, Y. De Koninck, B. Engelhardt, A. Prat, D. Côté, S. Lacroix, Neutrophils mediate blood-spinal cord barrier disruption in demyelinating neuroinflammatory diseases. *J. Immunol.* **193**, 2438–2454 (2014).
57. E. R. Pierson, C. A. Wagner, J. M. Goverman, The contribution of neutrophils to CNS autoimmunity. *Clin. Immunol.* **189**, 23–28 (2018).
58. J. R. Bradley, TNF-mediated inflammatory disease. *J. Pathol.* **214**, 149–160 (2008).
59. T. Tanaka, T. Kishimoto, Targeting interleukin-6: All the way to treat autoimmune and inflammatory diseases. *Int. J. Biol. Sci.* **8**, 1227–1236 (2012).
60. M. Yoshinaga, Y. Nakatsuka, A. Vandenbon, D. Ori, T. Uehata, T. Tsujimura, Y. Suzuki, T. Mino, O. Takeuchi, Regnase-1 maintains iron homeostasis via the degradation of transferrin receptor 1 and prolyl-hydroxylase-domain-containing protein 3 mRNAs. *Cell Rep.* **19**, 1614–1630 (2017).
61. S. Omiya, Y. Omori, M. Taneike, T. Murakawa, J. Ito, Y. Tanada, K. Nishida, O. Yamaguchi, T. Satoh, A. M. Shah, S. Akira, K. Otsu, Cytokine mRNA degradation in cardiomyocytes restrains sterile inflammation in pressure-overloaded hearts. *Circulation* **141**, 667–677 (2020).
62. K. N. Gibson-Corley, A. W. Boyden, M. R. Leidinger, A. M. Lambertz, G. Ofori-Amanfo, P. W. Naumann, J. A. Goeken, N. J. Karandikar, A method for histopathological study of the multifocal nature of spinal cord lesions in murine experimental autoimmune encephalomyelitis. *PeerJ* **4**, e1600 (2016).
63. A. J. Thompson, B. L. Banwell, F. Barkhof, W. M. Carroll, T. Coetzee, G. Comi, J. Correale, F. Fazekas, M. Filippi, M. S. Freedman, K. Fujihara, S. L. Galetta, H. P. Hartung, L. Kappos, F. D. Lublin, R. A. Marrie, A. E. Miller, D. H. Miller, X. Montalban, E. M. Mowry, P. S. Sorensen, M. Tintoré, A. L. Traboulsee, M. Trojano, B. M. J. Uitdehaag, S. Vukusic, E. Waubant, B. G. Weinshenker, S. C. Reingold, J. A. Cohen, Diagnosis of multiple sclerosis: 2017 revisions of the McDonald criteria. *Lancet Neurol.* **17**, 162–173 (2018).
64. H. Lian, E. Roy, H. Zheng, Protocol for primary microglial culture preparation. *Bio-protocol* **6**, e1989 (2016).
65. G. Matute-Bello, G. Downey, B. B. Moore, S. D. Groshong, M. A. Matthay, A. S. Slutsky, W. M. Kuebler, An official american thoracic society workshop report: Features and measurements of experimental acute lung injury in animals. *Am. J. Respir. Cell Mol. Biol.* **44**, 725–738 (2011).
66. T. P. Sheahan, A. C. Sims, S. R. Leist, A. Schäfer, J. Won, A. J. Brown, S. A. Montgomery, A. Hogg, D. Babusis, M. O. Clarke, J. E. Spahn, L. Bauer, S. Sellers, D. Porter, J. Y. Feng, T. Cihlar, R. Jordan, M. R. Denison, R. S. Baric, Comparative therapeutic efficacy of remdesivir and combination lopinavir, ritonavir, and interferon beta against MERS-CoV. *Nat. Commun.* **11**, 222 (2020).
67. T. Ashcroft, J. M. Simpson, V. Timbrell, Simple method of estimating severity of pulmonary fibrosis on a numerical scale. *J. Clin. Pathol.* **41**, 467–470 (1988).
68. Y. Hao, S. Hao, E. Andersen-Nissen, W. M. Mauck, S. Zheng, A. Butler, M. J. Lee, A. J. Wilk, C. Darby, M. Zager, P. Hoffman, M. Stoeckius, E. Papalexi, E. P. Mimitou, J. Jain, A. Srivastava, T. Stuart, L. M. Fleming, B. Yeung, A. J. Rogers, J. M. McElrath, C. A. Blish, R. Gottardo, P. Smibert, R. Satija, Integrated analysis of multimodal single-cell data. *Cell* **184**, 3573–3587.e29 (2021).
69. I. Korsunsky, N. Millard, J. Fan, K. Slowikowski, F. Zhang, K. Wei, Y. Baglaenko, M. Brenner, P. R. Loh, S. Raychaudhuri, Fast, sensitive and accurate integration of single-cell data with Harmony. *Nat. Methods* **16**, 1289–1296 (2019).
70. H. Wickham, D. Navarro, T. L. Pedersen, *ggplot2: Elegant Graphics for Data Analysis* (Springer-Verlag, ed. 2, 2016).
71. D. Kim, B. Langmead, S. L. Salzberg, HISAT: A fast spliced aligner with low memory requirements. *Nat. Methods* **12**, 357–360 (2015).
72. E. Afgan, D. Baker, B. Batut, M. van den Beek, D. Bouvier, M. Cech, J. Chilton, D. Clements, N. Coraor, B. A. Grüning, A. Guerler, J. Hillman-Jackson, S. Hiltemann, V. Jalili, H. Rasche, N. Soranzo, J. Goecks, J. Taylor, A. Nekrutenko, D. Blankenberg, The Galaxy platform for accessible, reproducible and collaborative biomedical analyses: 2018 update. *Nucleic Acids Res.* **46**, W537–W544 (2018).
73. P. D. Thomas, M. J. Campbell, A. Kejariwal, H. Mi, B. Karlak, R. Daverman, K. Diemer, A. Muruganujan, A. Narechania, PANTHER: A library of protein families and subfamilies indexed by function. *Genome Res.* **13**, 2129–2141 (2003).

Acknowledgments: We thank all members in Takeuchi laboratory for constructive comments; H. Yano (Ehime University) for providing BV2 microglia cells; K. Chen and D. Diez (Osaka University) for guidance of scRNA-seq analysis; H. Ueno and H. Yoshitomi (Kyoto University) for preparations of the scRNA library; Y. Sando, T. Kondo, T. Tsujimura, and S. Tarumoto for assistance with sequencing; and J. Hasegawa and Y. Okumoto for secretarial assistances. **Funding:** This work has been supported by grants from the Japan Society for the Promotion of Science (JSPS) KAKENHI (18H05278 to O.T. and 19H03488 to T.M.); JSPS of Science Grant-in-Aid JSPS Fellowship (19J23450 to K.M.T.); Grant-in-Aid for Transformative Research Areas (A) "Material Symbiosis" (20H05874 to T.U.); Japan Agency for Medical Research and Development (AMED) (JP20gm4010002, JP21ae0121030, and JP20fk0108454 to O.T.), and JSPS through the Core-to-Core Program. O.T. was funded by Astellas Pharma Inc., Takeda Science Foundation, and Uehara Memorial Foundation. **Author contributions:** K.M.T., X.C., T.M., and O.T conceived the study and designed the experiments; K.M.T., X.C., and T.M. performed the experiments and statistical analysis; K.M.T., A.V., T.U., and K.Y. performed scRNA-seq data acquisition and analysis; A.S. and T.T. performed the histology analysis; K.M.T., F.H., and M.Y. performed RNA-seq data acquisition and processing; M.K. and T.O. analyzed the patient samples; K.M.T. and O.T. prepared the manuscript; and O.T. supervised the project. All authors contributed to the critical revision of the manuscript. **Competing interests:** O.T. filed a patent application (PCT/JP2019/011851) (pending approval) regarding the use of antisense technology. All the other authors declare that they have no competing interests. **Data and materials availability:** All data associated with this study are available in the main text or the Supplementary Materials. The transcriptome and scRNA-seq data generated in this study are deposited in the Gene Expression Omnibus with accession numbers GSE182641 and GSE182646, respectively. Materials are available through a material transfer agreement by contacting O.T.

Submitted 20 January 2022
Accepted 21 April 2022
Published 11 May 2022
10.1126/scitranslmed.abo2137

Science Translational Medicine

Enhancement of Regnase-1 expression with stem loop–targeting antisense oligonucleotides alleviates inflammatory diseases

Ka Man TseAlexis VandenbonXiaotong CuiTakashi MinoTakuya UehataKeiko YasudaAyuko SatoTohru TsujimuraFabian HiaMasanori YoshinagaMakoto KinoshitaTatsusada OkunoOsamu Takeuchi

Sci. Transl. Med., 14 (644), eabo2137. • DOI: 10.1126/scitranslmed.abo2137

A *Regnase-1* remedy

Regnase-1 is an RNase known to limit inflammation by targeting specific mRNAs through recognition of stem-loop (SL) structures in 3# untranslated regions. Tse *et al.* now describe a therapeutic approach of blocking Regnase-1 self-regulation to limit inflammatory responses. They targeted the binding interaction between Regnase-1 and SL structures using two antisense phosphorodiamidate morpholino oligonucleotides (MOs), which enhanced Regnase-1 expression in macrophages and, in turn, reduced expression of proinflammatory transcripts targeted by this RNase. Tissue-targeted delivery of Regnase-1–specific MOs attenuated acute respiratory inflammation and chronic fibrosis in the lung and experimental autoimmune encephalitis symptoms in the nervous system. Regnase-1 expression also inversely correlated with multiple sclerosis disease severity in patients. These findings highlight a role for Regnase-1 in inflammatory diseases and suggest potential therapeutic benefits of targeting this mechanism.